# Non-uniform dune development in the presence of standalone beach buildings

Vos, Sander; van IJzendoorn, Christa; Lindenbergh, Roderik; de Wulf, Alain

**DOI**
10.1016/j.geomorph.2024.109402

**Publication date**
2024

**Document Version**
Final published version

**Published in**
Geomorphology

**Citation (APA)**
Vos, S., van IJzendoorn, C., Lindenbergh, R., & de Wulf, A. (2024). Non-uniform dune development in the presence of standalone beach buildings. *Geomorphology*, *466*, Article 109402. https://doi.org/10.1016/j.geomorph.2024.109402

Geomorphology 466 (2024) 109402

Contents lists available at ScienceDirect

Geomorphology

journal homepage: www.journals.elsevier.com/geomorphology

# Non-uniform dune development in the presence of standalone beach buildings

Sander Vos [a,d,*], Christa van IJzendoorn [b], Roderik Lindenbergh [c], Alain de Wulf [d]

[a] Delft University of Technology, Faculty of Civil Engineering and Geosciences, Department of Hydraulic Engineering, Stevinweg 1, 2628CN Delft, the Netherlands
[b] Oregon State University, College of Earth, Ocean, and Atmospheric Sciences, 104 CEOAS Admin Building, Corvallis, OR 97331-5503, USA
[c] Delft University of Technology, Faculty of Civil Engineering and Geosciences, Department of Geoscience and Remote Sensing, Stevinweg 1, 2628 CN Delft, the Netherlands
[d] Ghent University, Department of Geography, Krijgslaan 281 S8, 9000 Ghent, Belgium

ARTICLE INFO

*Keywords:*
Aeolian sediment transport
Urbanized beaches
Dune development
Laser scanning

ABSTRACT

Shoreward sand transport and dune development are increasingly influenced by the urbanization of beach-dune systems in the Netherlands. Three topographic datasets, on various spatio-temporal scales, are used to study the effect of standalone buildings on long term local dune development. On the smallest scale, terrestrial laser scans are used to study the geomorphological effects of two sea containers on the beach. On the intermediate scale, the geomorphological effects of a beach pavilion on the local dune development are studied with a 2-year topographic dataset of (bi) monthly permanent laser scans. Finally, 15 yearly airborne lidar scans of the beach-dune system in Noordwijk are used to evaluate the effect of multiple beach pavilions on dune growth variations. The small-scale experiment shows that horseshoe-shaped deposition patterns developed on the leeside of the containers. These depositions follow daily wind changes and leave deposits corresponding to the residual wind direction over the whole measuring period. Similar patterns are found around the larger beach pavilion, but anthropogenic activities like bulldozing and beach shaping make the determination of the effect on dune development harder to discern. Evaluation of the longer-term dataset reveals large variations in dune height and volume around beach pavilions. Dune height/volume increases vary between 1 and 8 m in height and 0–200 m3 in volume. A variability analysis shows that the length scale of alongshore variability in dune height/volume of urbanized dunes can be 10 times smaller than for natural dunes. For about half the beach pavilions, variations in dune height and volume are significantly correlated to the location of beach pavilions but correlation to particular beach pavilion properties is yet inconclusive.

## 1. Introduction

Coastal dune systems occur at many locations around the world where deposited sand is blown inland and accumulates onshore around anchor points like vegetation, pebbles, or other objects (Hesp, 1989). The dunes contribute to society by fulfilling various ecosystem functions (Wijnberg et al., 2021) like drinking water storage/filtering, ecological refuge, tourism, and protection of urbanized low-lying hinterlands. Shoreward sand transport is one of the main drivers of natural dune development and coastal resilience. This process is highly dynamic in nature and dependent on marine and aeolian forcing. Tides and waves transport sand landwards via incoming intertidal sand bars during mild weather conditions (Masselink et al., 2006; Vos et al., 2020) and wind-driven transport moves sand in landward direction towards the dunes (Hoonhout and de Vries, 2017).

Human or anthropogenic interventions on sandy beach dune systems have existed for many decades (Nordstrom, 1994; Flor-Blanco et al., 2013; Huang and Jin, 2018), with some measures like marram grass planting going back for centuries (Viborg, 1788). Especially in the last decades, an increasing urbanization of beaches has been observed in various countries (Malavasi et al., 2013; Hoonhout and Waagmeester, 2014). In Western Europe, many seasonal and permanent beach pavilions, clubs, and recreation/holiday buildings are present along the beach-dune interface (Fig. 1). These types of buildings are especially prevalent in the Netherlands, where beach housing has increased with a factor 20 in the last 15–20 years (van Bergen et al., 2021). This is

* Corresponding author at: Delft University of Technology, Faculty of Civil Engineering and Geosciences, Department of Hydraulic Engineering, Stevinweg 1, 2628CN Delft, the Netherlands.
*E-mail address:* s.e.vos@tudelft.nl (S. Vos).

https://doi.org/10.1016/j.geomorph.2024.109402
Received 21 December 2023; Received in revised form 23 August 2024; Accepted 23 August 2024
Available online 3 September 2024

accompanied by an increase in anthropogenic activities (like bulldozing, beach shaping and beach cleaning) to maintain beaches and beach housing accessibility (Jackson and Nordstrom, 2011; Nordstrom et al., 2007). The effects of anthropogenic activities over longer time periods are not easily visible and quantifiable, which limits the determination of relevant processes and their associated time scales.

Beach buildings can influence aeolian sediment transport (García-Romero et al., 2016; Morton et al., 1994; Hallin et al., 2019), can change the shape of the dune (Nordstrom and McCluskey, 1985), and reduce the chance of a positive dune volume trend (Hoonhout and Van Thiel de Vries, 2013).

A long-term reduction in aeolian transport towards the dunes might locally affect coastal resilience (Masselink and Lazarus, 2019). Research by Poppema et al. (2021, 2022a, 2022b) and Pourteimouri et al. (2022, 2023) has focused on the effect of building properties (like geometry, spacing and orientation) on the wind flow/aeolian sediment deposition at scales of hours to years. The translation from monthly/yearly morphological development around isolated buildings to decadal dune development on adjacent coast has received little attention. An integral view across temporal and spatial scales is needed to determine whether buildings affect decadal coastal dune development.

Three topographic datasets that cover a range of spatial and temporal scales are used to analyze the cumulative effect of the presence of buildings over time and space. The first dataset covers a 3-month field campaign (Scanex2020, Poppema et al., 2021) on a spatial scale of 100 m to study the influence of a simplified building on aeolian sand depositions. The second dataset contains data of a 2-year field study covering ~500 m (CoastScan project, Vos et al., 2017, 2023) to determine the influence of a single beach pavilion in front of a dune on longer term dune development. Finally, a 15 year dataset of yearly airborne lidar scans is used to study the alongshore dune variability due to multiple beach pavilions along a 2.7-km stretch of coast.

The field site is located in Noordwijk, the Netherlands where 17 standalone buildings are present in front of the dune system (Fig. 2). The beach-dune system in Noordwijk was altered in 2008 which provides a unique starting point to analyze long-term dune development. Alongshore variations in dune development in Noordwijk are compared to those of natural dune systems in the Netherlands to distinguish the effect of buildings from natural variations in dune development (e.g., de Winter et al., 2015; Houser, 2013).

## 2. Field site

### 2.1. Noordwijk

Noordwijk (52.244° N, 4.430° E, the Netherlands, see Fig. 2) is a former fishing village which transitioned to a seaside resort around the 1900s. For a long time, this sea-side village was a weak link in the protective function of the Dutch coast. In 2007/2008 the coastal protection was upgraded by implementing a 'dike in a dune' solution at the sea boulevard (Almarshed et al., 2020). The dune front was extended and reshaped approximately 50 m seaward of its initial position which can be seen in Fig. 2A and C. Fig. 2B shows the development of the cross-shore profile just south of the boulevard (indicated with a red dashed line in 2A) based on yearly coastal profile measurements (Jarkus dataset, van IJzendoorn et al., 2021). It shows the extension and the natural dune development after the redesign of the coast in 2008.

The beach-dune system around Noordwijk is orientated from south-southwest to north-northeast. Dune heights vary between +10 to +24 m above mean sea level. Sand consists of quartz sand with a median grain size (D50) of around 300 μm (van IJzendoorn et al., 2023) and patches of shells on the surface. Vegetation in the dunes consists among others of marram grasses (Ammophila) and sea buckthorn with marram grasses favoring areas closer to the sea. The beach-dune system is driven by

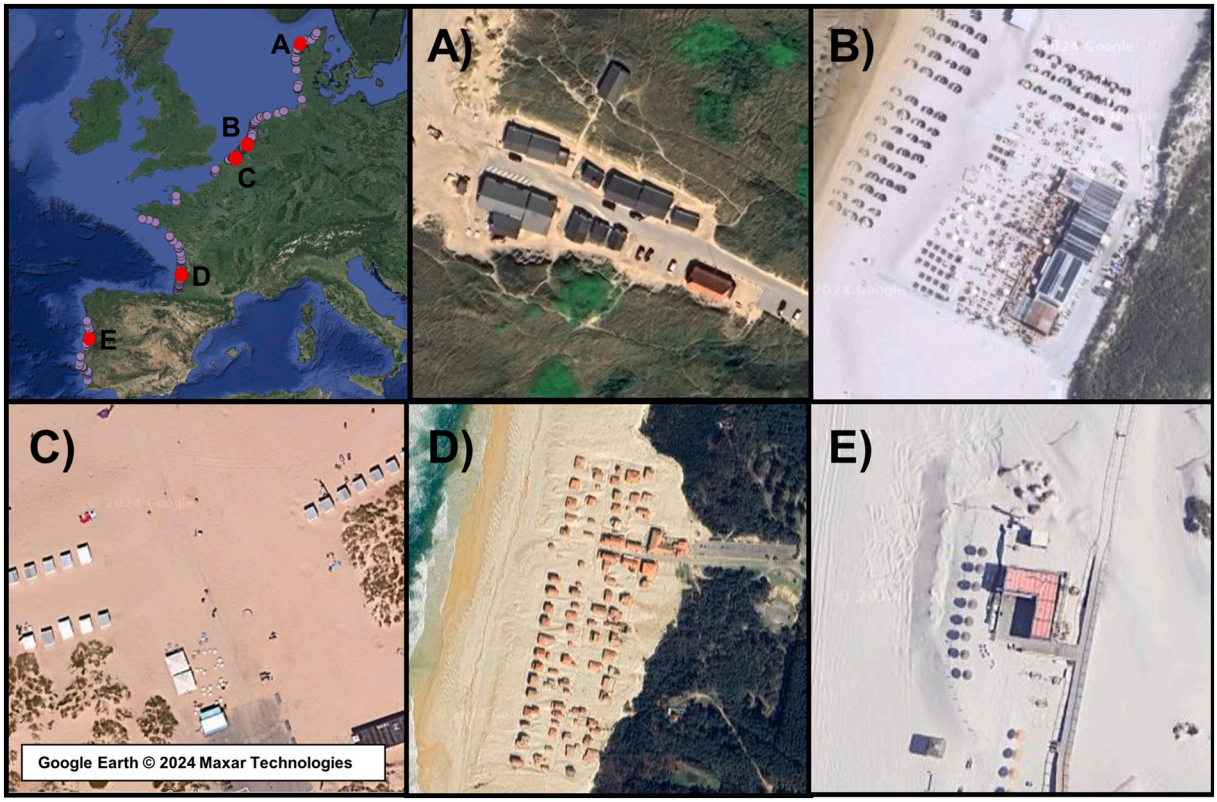


**Fig. 1.** Overview of beach buildings in Western Europe based on Google satellite data (2024) with examples of beach buildings in A) Denmark (56.9298°N, 8.3377°E), B) The Netherlands (52.2377°N, 4.4218°E), C) Belgium (51.1295°N, 2.6562°E), D) France (43.9510°N, 1.3632°W) and E) Portugal (40.6315°N, 8.7493°W). This article will focus on beach buildings including and around the building shown in B).

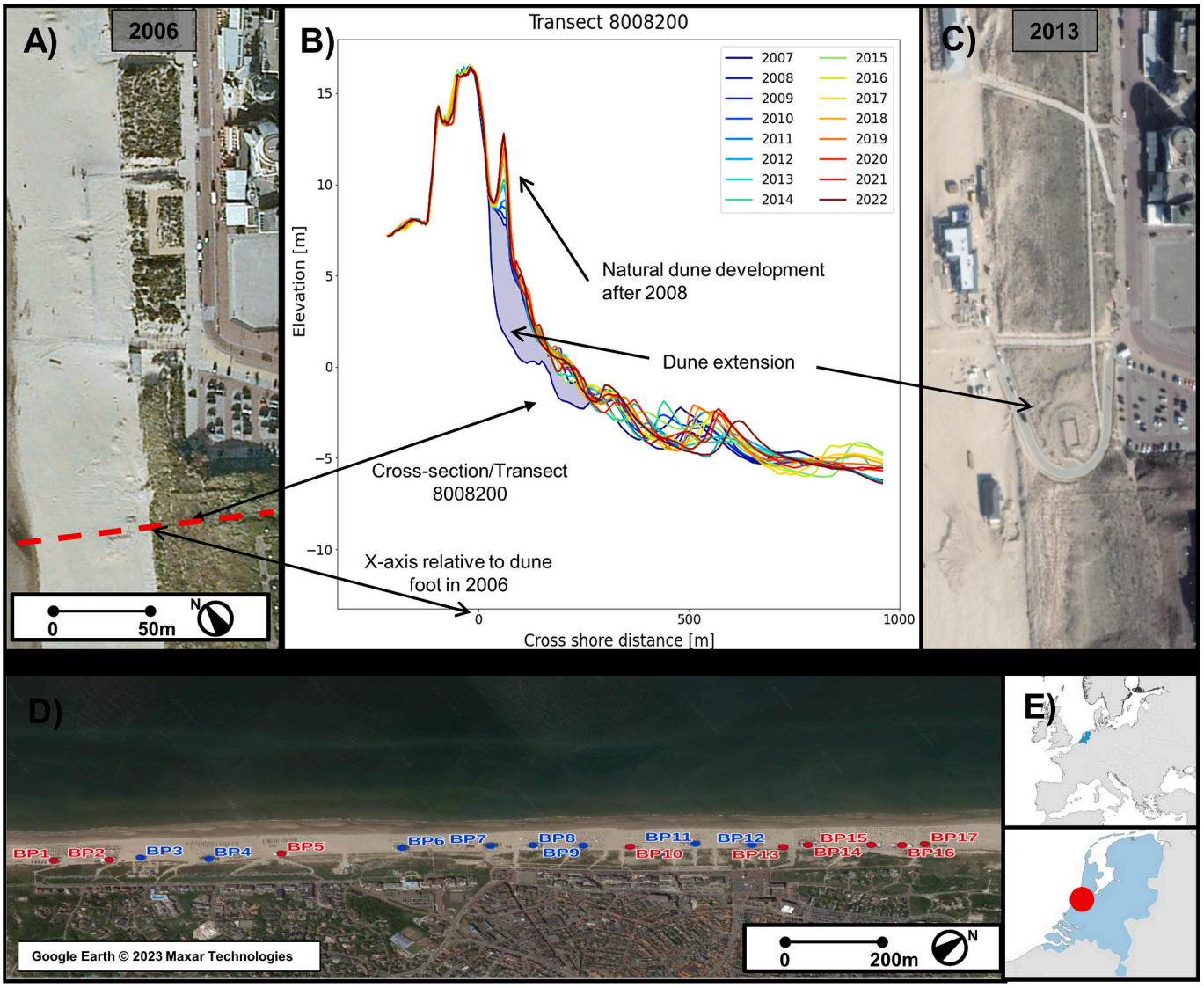


**Fig. 2.** Dune development and beach pavilions at Noordwijk, The Netherlands. Panel A and C show the development (2006–2013) after the artificial seaward extension in 2008 of the dune in front of the old dune row. The red dashed line in 2A indicates the cross-section shown in 2B which shows the natural development of the dunes from 2008 to 2022. The x-axis is relative to the dune toe in 2006. The locations of 17 beach pavilions (seasonal beach pavilions in red and permanent beach pavilions in blue) along the village beach are indicated in Panel D. The location of the red cross-section in Panel A is just north of BP7 in Panel D. Finally Panel E shows the location of Noordwijk within the Netherlands.

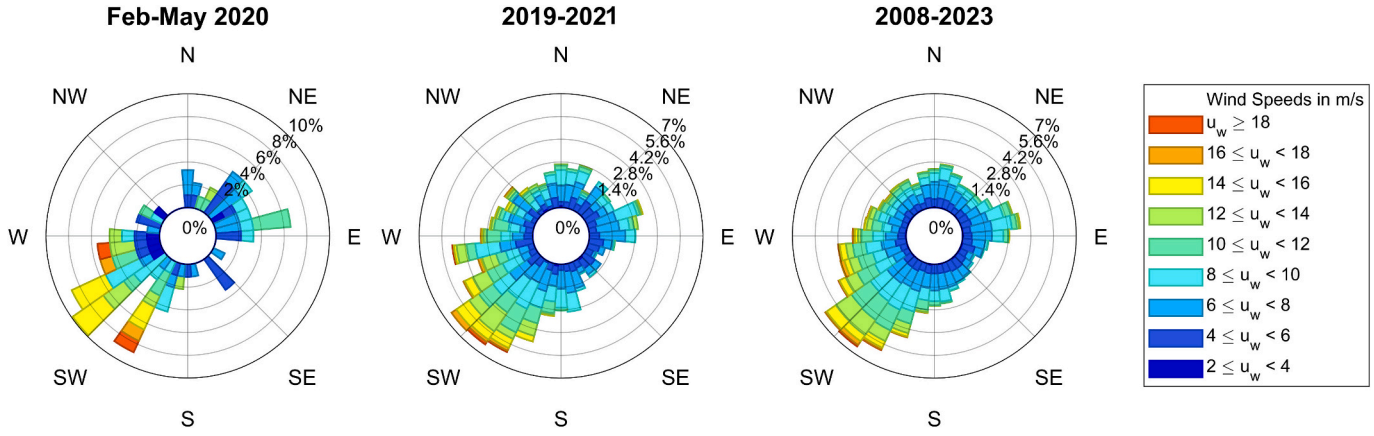


**Fig. 3.** Wind rose of the wind conditions at Noordwijk (based on nearest coastal measurement location IJmuiden at 52.462°N, 4.555°E, KNMI, 2024), the Netherlands for the (A) Scanex2020 and (B) CoastScan field campaign and (C) the long-term analysis from 2008 until 2023.

average 1.7-m waves from SW-NW, with the smaller (significant wave height $H_s < 1$ m) and largest waves ($H_s > 5$ m) from the W-NW direction (Luijendijk et al., 2017). Tides at Noordwijk are semidiurnal and asymmetric (rising/falling period of about 5/7 h) with a spring/neap tidal range of about 1.8/1.4 m (Wijnberg, 2002).

### 2.2. Wind conditions

During the Scanex2020 field campaign (Fig. 3), winds were dominantly from the southwest and easterly direction. Several storms occurred in the beginning of the experiment with maximum wind speeds above 20 m/s while the second period was relatively quiet with easterly wind speeds below 10 m/s. Wind statistics over the longer time periods stabilize to a south-western dominated wind field. In general, most high wind speeds from this direction are associated with incoming storms from the west, while the easterly winds are connected to stable weather due to high pressure systems on mainland Europe.

### 2.3. Beach buildings and anthropogenic activities

The urbanized beach approximately follows the village limits of Noordwijk (see Fig. 2D). A total of 17 beach pavilions/ buildings (hereafter referred to as beach pavilion and abbreviated as BP) are located around the 2.7-km-long dune foot (Table 1). The BP's can be reached via 17 beach access paths. The BPs are either permanent (8 in total) or seasonal (9 in total). Seasonal BPs are constructed around the end of March and removed at the end of October. The BPs are of similar dimensions (maximum square footage for the building and terraces are 600 and 400 $m^{2,}$ respectively) as prescribed by the local municipality. The estimated height and cross section width (perpendicular to the main wind direction) show variations of 4–6 m in height and 10–35 m in width.

The beach pavilions are positioned on sand embankments of about 30 m in cross-shore direction and 90 m in alongshore direction in front of the dune. Unofficial embankments are created on the beach for seating areas and temporary protection in front of the BPs against storms. Other anthropogenic activities include dune entrance cleaning, beach cleaning/shaping and large-scale transport (i.e. for the (de)construction of the seasonal BPs). Although some measurements (Barbero-García et al., 2023) are available about the anthropogenic activities on the beach, these encompass only a couple of days during the Scanex2020 field campaign and only around BP6. Other information about anthropogenic activities is only circumstantial and derived from, for example, the yearly deconstruction/construction of BPs and the creation of embankments for seating areas and storms.

## 3. Elevation data collection and analysis

### 3.1. Terrestrial Laser Scanning (order 100 m)

For this paper, elevation data from different experiments and sources were combined (Vos et al., 2024). On the smallest scale (Order 100 m), Terrestrial Laser Scan (TLS) measurements are available from the Scanex2020 campaign in 2020 (Poppema et al., 2021; Hallin et al., 2023). During the experiment, two sea-containers were placed on the beach to study the impact of a simplified building on aeolian sediment transport (Fig. 4A-B) and the accumulative effect on local dune development. The (Bi)weekly TLS measurements (Fig. 4C) were obtained with a Leica P30 (Table 2). On average three scans (with about 10.000.000 points each) were made to cover the field area per scan epoch. The scans were georeferenced to fixed objects around the scan area (the hotel, the beach pavilion [BP6] and the local sailing club [BP7]). The earliest TLS scans were referenced against coordinates of PLS measurements (Section 3.2) collected at the same time. Consecutive TLS scans were referenced against the coordinates of objects in the first TLS scans. After registration, the TLS data were gridded on a 1*1 m grid for analysis.

### 3.2. Permanent Laser Scanning (order 500 m)

On a medium scale (Order 500 m), 2 years (2019–2021) of scans were used from the Permanent Lasers Scan (PLS) setup in Noordwijk (Fig. 2D and E) (CoastScan, Vos et al., 2023). The scans monitored the beach and dunes during the CoastScan experiment to study the inter-annual variability of the beach and dunes. A Riegl VZ-2000 terrestrial laser scanner (Table 2) was positioned on top of a hotel scanning the beach hourly for a three-year period (Kuschnerus et al., 2023; Vos et al., 2023). Scans contained on average 8 million points over a 1000 × 300 meter beach-dune area. Measurements were supplemented (bi)monthly with TLS measurements (from 2019 till 2021) north and south of BP6 to fill shadows in the PLS scans.

The location of the laser scanner was determined with 6 reflectors (Ø 5 cm) on both the hotel and objects around the hotel. They were spread over a 180-degree window in the field of view and positions were obtained using RTK-GNSS (real-time kinematic global navigation satellite system measurements). A global transformation matrix (translation and rotation) from local point coordinates to the Dutch reference system (RD-NAP, EPSG 28992, [de Bruijne et al., 2005]) was determined using RiSCAN Pro (Riegl, 2023). Due to a move of the laser scanner on 2nd

**Table 1**
Overview of the beach pavilions in Noordwijk. All pavilions started as seasonal (S) pavilions, but several became permanent (P, with the year of change indicated between brackets) since 2008. Some pavilions were also either enlarged or moved since 2008. The distance between the beach pavilions is given in meters. The height and cross-section width (width of the pavilion perpendicular to the main SW wind direction) of the pavilions are estimated using airborne lidar surveys of 2021–2023. Some seasonal pavilions (indicated with *) were not yet constructed during the airborne surveys conducted in the spring.

| Beach pavillion | Type (year) | | Latitude | | Longitude | | Distance (m) | Height (m) | Cross-section (m) | Comments |
|---|---|---|---|---|---|---|---|---|---|---|
| BP1 | S | | 52.2341 | °N, | 4.4194 | °E | 0 | 4 | 25 | |
| BP2 | S | | 52.2352 | °N, | 4.4204 | °E | 143 | 5 | 20 | |
| BP3 | P | (2019) | 52.2360 | °N, | 4.4209 | °E | 115 | 4 | 10 | Moved 30 m north 2019 |
| BP4 | P | (2011) | 52.2375 | °N, | 4.4225 | °E | 182 | 5 | 15 | Enlarged 2011 |
| BP5 | S | | 52.2391 | °N, | 4.4235 | °E | 195 | 5 | 20 | Enlarged 2016 |
| BP6 | P | (2010) | 52.2418 | °N, | 4.4254 | °E | 337 | 5 | 20 | |
| BP7 | P | (2008) | 52.2438 | °N, | 4.4270 | °E | 203 | 6 | 20 | New building 2021 (50 m north) |
| BP8 | P | (2014) | 52.2448 | °N, | 4.4280 | °E | 166 | * | * | |
| BP9 | P | (2011) | 52.2457 | °N, | 4.4288 | °E | 130 | 5 | 25 | |
| BP10 | S | | 52.2468 | °N, | 4.4299 | °E | 136 | * | * | |
| BP11 | P | (2010) | 52.2482 | °N, | 4.4311 | °E | 178 | 5 | 20 | |
| BP12 | P | (2010) | 52.2495 | °N, | 4.4322 | °E | 156 | 8 | 30 | |
| BP13 | S | | 52.2502 | °N, | 4.4330 | °E | 99 | * | * | New 2014 |
| BP14 | S | | 52.2508 | °N, | 4.4333 | °E | 62 | 5 | 35 | New 2018 |
| BP15 | S | | 52.2521 | °N, | 4.4346 | °E | 173 | 5 | 25 | Enlarged 2013 |
| BP16 | S | | 52.2529 | °N, | 4.4354 | °E | 97 | 4 | 20 | Enlarged in 2013/2018 |
| BP17 | S | | 52.2533 | °N, | 4.4358 | °E | 49 | * | * | |

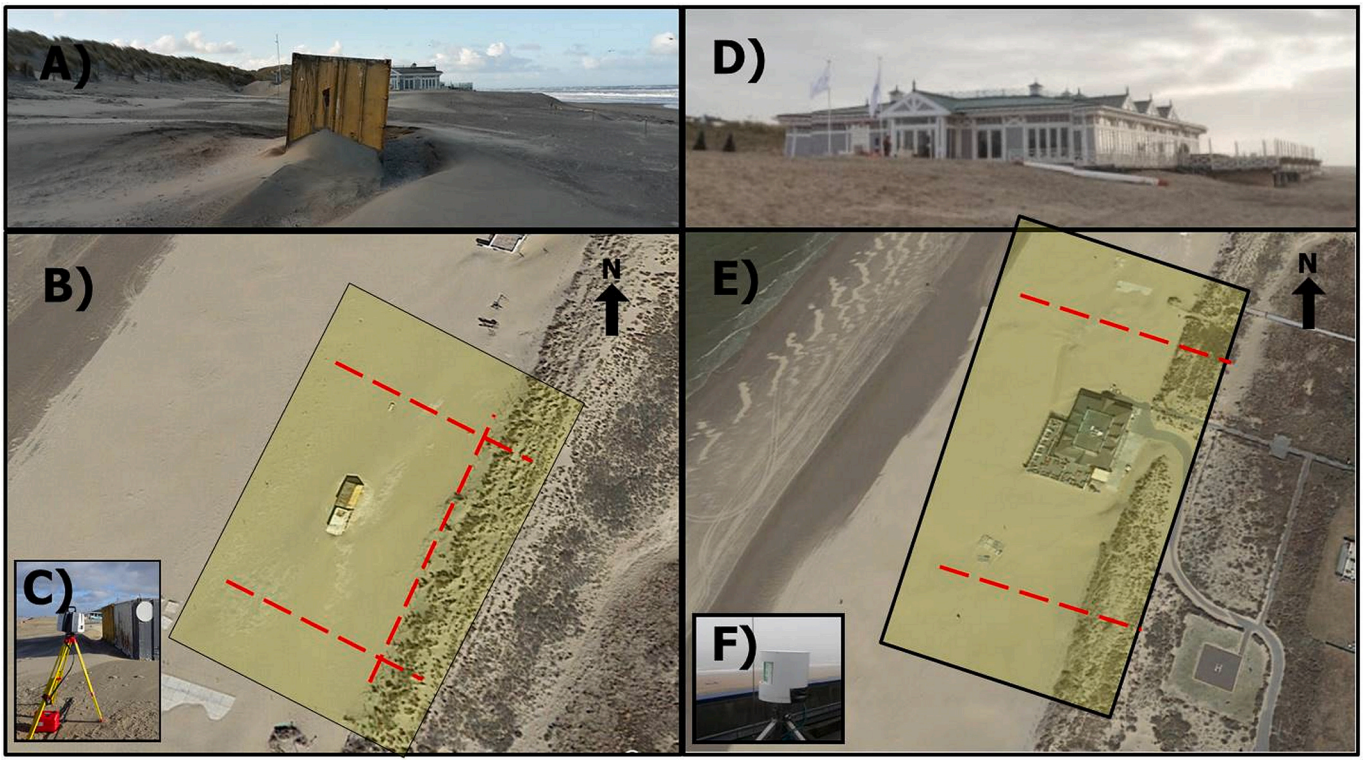


**Fig. 4.** Scanex2020 and CoastScan field campaign in Noordwijk. Scanex2020 (4A-4B) was conducted from Jan-Apr 2020 to determine the impact of buildings on aeolian sand transport and local dune development. Measurements were obtained (bi) weekly with a terrestrial laser scanner (4C). CoastScan was conducted from June 2019–July 2021 to determine the natural variability of the sandy coast around BP6 (4D-E). Measurements were obtained (bi) monthly with a permanent laser scanner (4F) and an additional terrestrial laser scanner. Red lines indicate cross-sections used in the analysis for Scanex2020 (4B) and CoastScan (4E).

**Table 2**
Laser scan specifications and overview of measurements in measurement sets.

| Scanner | Range | Accuracy | pnts/s | pnts/m2 | Scan interval | Scanex2020 | CoastScan | Noordwijk |
|---|---|---|---|---|---|---|---|---|
| TLS: Leica-P30 | 270 m | 6 mm at 100 m | 400,000 | 5 at 100 m | (Bi)weekly/monthly | 33 scans | 48 scans | – |
| PLS: Riegl-VZ2000 | 2000 m | 8 mm at 150 m | 21,000 | 5 at 300 m | Monthly | – | 24 scans | – |
| ALS: Various | – | – | – | 0.04/1 | Yearly | – | – | 16 scans |

December 2020, a recalibration was performed with the same reflectors after the move. The move and several other removals of the laser scanner for maintenance have resulted in small displacements of the measurement frame. To correct these, each scan is corrected separately with a time dependent correction. This also addresses slight variations of the internal inclination sensor over time.

Individual laser scans were corrected with a time dependent rigid (rotation) transformation matrix by comparing 2 fixed georeference objects in the $N^{th}$ scan with the same objects in the first scan. The rotation of the scan (around the X- and Y axis) was calculated by minimizing the vertical distance between the scan data at the georeferenced objects (in local coordinates) as expressed in Eq. (1):

$$\begin{cases} (\Delta\Phi, \Delta\Psi) = minimise(J) \\ J = \sum (Z_{scan} - Z_{obs})^2 \end{cases} \quad (1)$$

Here, ΔΦ and ΔΨ are the angle corrections found for the X- (towards the sea) and Y-axis, J is the cost function and $Z_{scan}$ and $Z_{obs}$ are the height of the reference objects in the scan. The reference objects consisted of the roof of the beach pavilion (BP6) in front of the hotel (X-axis rotation) and a concrete floor (part of a footpath, 52.2435°N, 4.4279°E) north of the laser scanner (Y-axis rotation). Fig. 5 gives the results for the X-axis (Fig. 4A) and Y-axis (Fig. 4B) time dependent corrections for the (bi) monthly scans found with the time dependent correction method. It shows the average height at the reference areas before and after corrections. The method reduced the range from about 0.5 m to within 5–10 cm.

(Bi)monthly TLS measurements were used to fill gaps caused by shadow effects in certain PLS measurements. The dune front north and south of BP6 were surveyed from July 2019–November 2021 and were obtained to fill in gaps (especially the dune toe) obtained from the PLS. The TLS measurements were also referenced to the hotel, beach pavilion and local sailing club. The TLS and PLS scans were combined to obtain a full grid at 1 × 1 meter resolution. An example of the merge can be seen in Fig. 6 which shows a grid of the beach-dune systems around BP6 with either TLS or PLS sources indicated by colour. The figure shows a grid in local coordinates (of the PLS) with PLS measurements in blue and TLS measurements at two different locations indicated in green and red.

### 3.3. Airborne lidar scanning (order >1000 m)

On the largest scales (Order 3000 m), data was obtained from governmental repositories owned by Rijkswaterstaat (RWS), Ministry of Infrastructure and Water Management, the Netherlands (RWS, 2023). The Dutch Coast has been regularly monitored since the early 1960's. In the early days, multiple techniques were used to obtain cross-sections along the coast at a regular interval (van IJzendoorn et al., 2021; de Vries et al., 2012). Since the 2000's the coast has been completely covered with airborne lidar measurements (Sallenger Jr. et al., 2003).

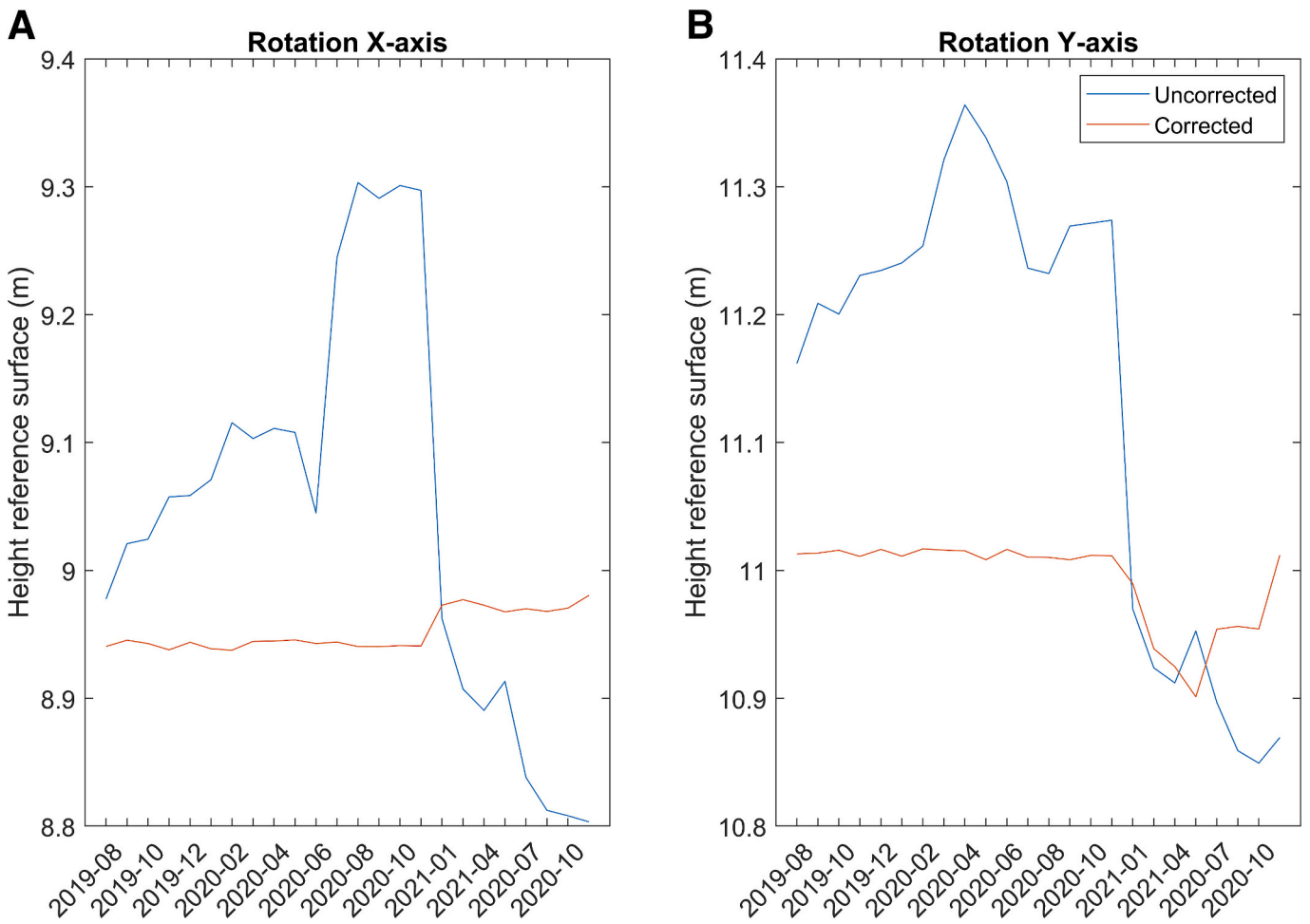


**Fig. 5.** A, B. Heights of the reference areas for the X (roof of the beach pavilion BP6) and Y (footpath) axis rotation before and after the time dependent correction.

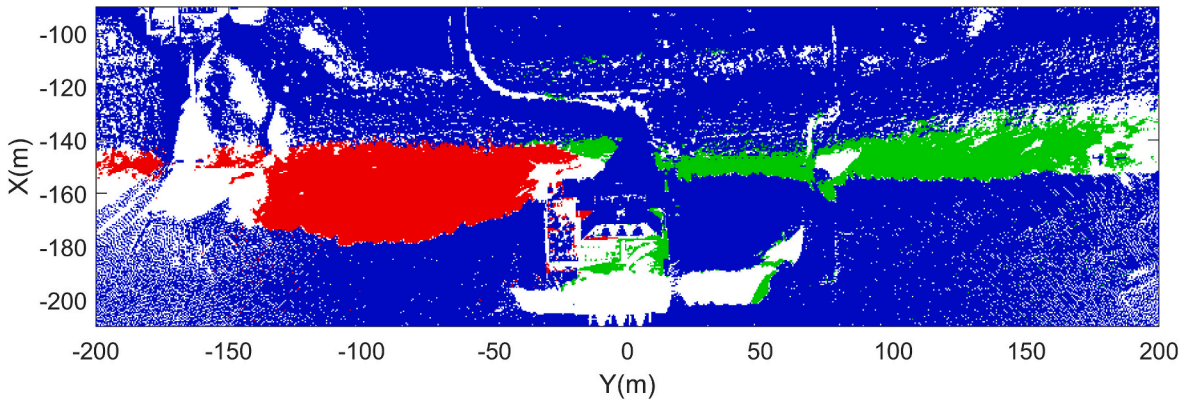


**Fig. 6.** Grid filled with PLS/TLS scan data with individual scans indicated by colour. PLS points are dark blue while the red and green colour indicate individual TLS scans measured at two different locations around BP6 (see Fig. 2D-E). The grid is in local coordinates of the PLS (with the center point of the axis at the base of the laser scanner) with negative X values directed towards the sea and positive Y coordinates alongshore the coast in NE direction. The beach pavilion is located X = -180 m and Y = 0.

For this analysis, 5 × 5 meter georeferenced geotiff grids with beach-dune terrain heights up till 2012 were used while georeferenced 'laz' point cloud files were used for later years. Over time, the resolution of the 'laz' files has increased to about 5–10 points per $m^2$ in 2023. All files are converted via triangulation to a 1 × 1 grid (meaning interpolation of data up to 2012) for further analysis.

### 3.4. Effect of dune vegetation on elevation measurements

A large part of the dunes in Noordwijk is covered with vegetation like marram grasses and sea buckthorn. This vegetation is expected to affect the elevation measured with laser scanning techniques. Several methods are available to remove vegetation from laser scans (Evans and Hudak, 2007; Chehata et al., 2008; Zhang and Lin, 2013; Dandois and Ellis,

2013), however, these techniques have not been applied to the TLS/PLS and ALS data in this study. For the ALS data, not enough information is available to accurately remove the vegetation. Up to 2012, only 5 × 5-meter geotiff files are available, which do not provide much detail about the presence of vegetation. Similarly, the airborne lidar data after 2012 contain too few points per $m^2$ to effectively determine the difference between a plant and the bottom. For the PLS data, the dot size of the laser around the vegetation was too large to obtain sufficient information of the ground under the vegetation. Removing the vegetation would result in large gaps in the point cloud data and filling these gaps by interpolating would create additional errors.

Airborne lidar has been used to map vegetation in dune areas (Hantson et al., 2012, Kathmann et al., 2022) with vertical average errors up to 30–40 cm depending on the surface and/or vegetation. This is similar to results obtained in other landscapes which give errors of 30–50 cm (Anders et al., 2019; Coveney and Fotheringham, 2011; Hantson et al., 2012). As the point clouds don't provide enough points to remove vegetation, the vertical error of the dune height measurements in this article is estimated at about 30 cm. This estimate is based on visual observations of vegetation height in the field. For non-vegetated areas like the beach a maximum vertical error of about 5 cm is considered based on research with the PLS laser scanner in Kijkduin, The Netherlands (Vos et al., 2022).

### 3.5. Extraction of dune properties from elevation measurements

Dunes are often defined based on their morphology (Hesp and Walker, 2013; Tsoar et al., 2004), but the definitions describing the dune properties can be inconsistent (Wernette et al., 2018) as the exact location of the dune toe/top/heel can be subjective. To make a consistent comparison of the dune development between different alongshore locations at Noordwijk beach, different dune properties were predefined, extracted and analyzed. In this study, the definitions of Wernette et al. (2018) for dune toe/top/heel are used and a modified method based on the Jarkus Analysis Toolbox (van IJzendoorn et al., 2021) was used to determine the location of the dune toe/top/heel.

The dune top (blue line in Fig. 7) was determined in a two-step approach. The primary dune top was defined as the most seaward dune top that has a height that is larger than 6 m and a prominence that is larger than 0.5. The prominence of a peak measures how much a peak stands out and is defined as the vertical distance between the peak and its lowest surrounding contour line. The dune top was determined at 26

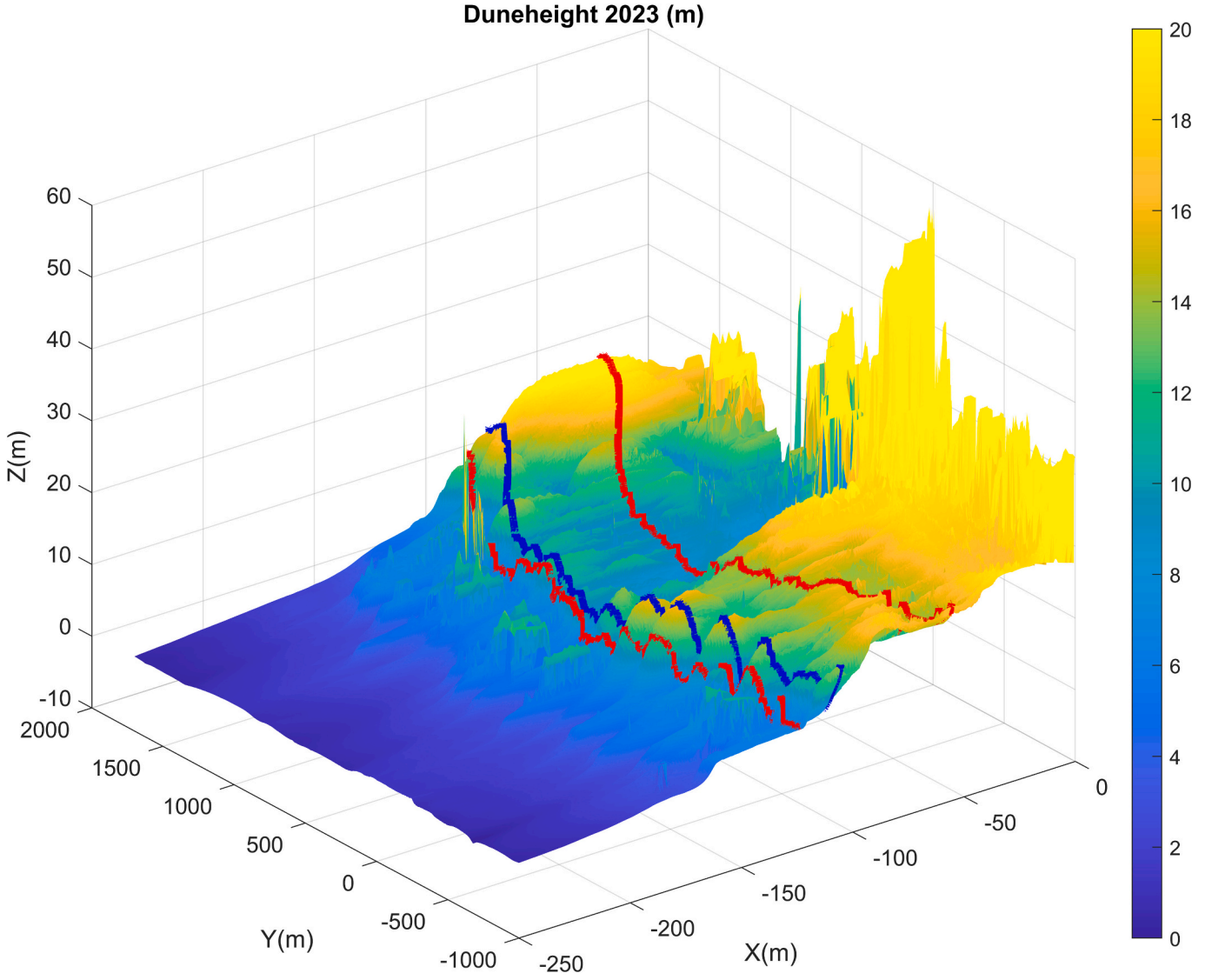


**Fig. 7.** The dune toe/top/heel locations that are used to extract the temporal dune development trend from the 15-year airborne lidar dataset. The dune top is shown in blue while the dune toe (seawards) and dune heel (landwards) are shown in red. It should be noted that the dimensions in the plots are skewed to improve the visibility.

cross-sections spread over the grid (from south to north with a step size of 100 m). Locations with no clear dune growth (for examples dune entrances) were skipped. Finally, for certain alongshore locations no clear dune top could be determined in a cross-section with the dune top routine (due to the prominence rule). In these cases, dune top locations were determined by identifying locations in the cross-section visually with the largest dune growth.

The dune toe location (left red line in Fig. 7) is based on the 2nd derivative method of Diamantidou et al. (2020). As this method is based on natural dune profiles, an adaptation was necessary to incorporate the sand embankments of the BPs. Our method searches the dune toe seawards of the dune top and defines the dune toe location when either the 1st and 2nd derivatives are $<0.01$ (m/m for the 1st derivative and m/m$^2$ for the 2nd derivative) or when the dune height is lower than 6 m. The dune toe routine was applied to the same cross-sections as the dune top routine.

The dune profile in Noordwijk has no clear dune heel due to buildings and other hard surfaces in the dune area. For volume analysis the dune heel was defined 50 m landwards of the dune top. Here it was assumed that the dune profile does not change significantly as can be seen in Fig. 2B. The results of the determination of the dune heel, toe and top are shown in Fig. 7 which shows the dune map (of 2023) with the dune top indicated in blue and the dune toe (seaward) and heel (landwards) indicated in red. A 7th order polynomial fit through each of the cross-shore dune parameters (dune toe, top and heel) was used to obtain continuous alongshore lines.

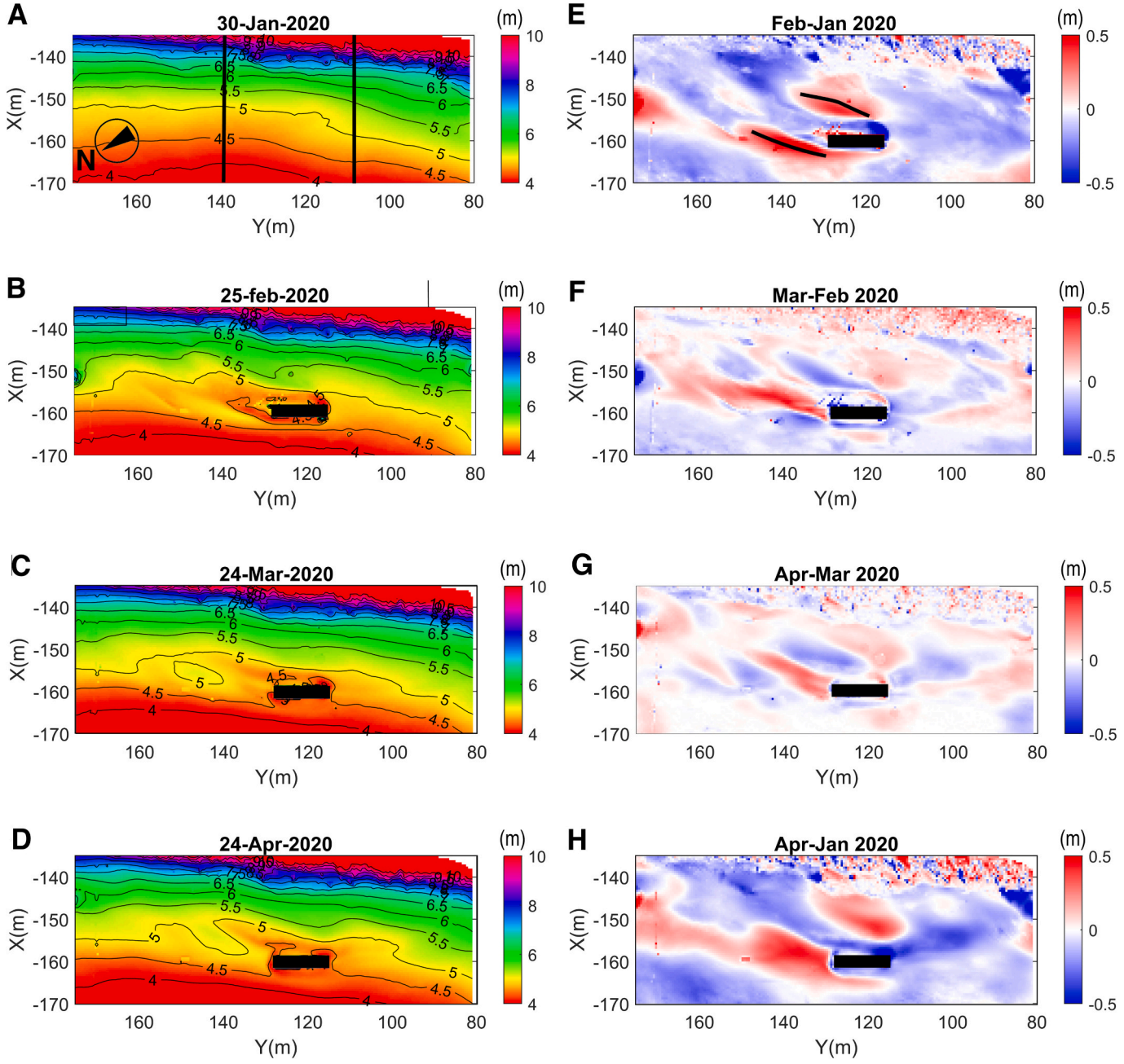


**Fig. 8.** Evolution of the beach and dune toe around a container (black rectangle) for 3 months in 2020. Panels A-D shows the monthly beach/dune heights in meters. Panels E-G shows the month-to-month change in meters, while Panel H shows the overall changes in four months. The arrow in the first image indicates the orientation of the beach to north and the black line in Panel E indicates the general shape of the horseshoe deposition pattern. The black lines in Panel A indicate the cross-sections in Fig. 4A and B. The along-section in Fig. 4C is along X = −140 m.

### 3.6. Analyzing alongshore variations in dune development

Dune systems show natural alongshore variations and strong variations in the alongshore could result in local reduced coastal resilience. To analyze systematic spatial variations in the alongshore dune height and dune volume a spatial autocorrelation can be used (de Vries et al., 2012). The autocorrelation R is here defined as

$$R_\tau = \frac{\sum (X|dune(y) - \overline{X}_{dune})^*(X_{dune}(y+\tau) - \overline{X}_{dune})}{\sum (X|dune(y) - \overline{X}_{dune})^2} \quad (2)$$

with X either representing the dune height or volume and $\tau$ the autocorrelation length (Moran, 1950). The autocorrelation length is dependent on the spatial spreading of the correlation of dune development along the coast. For example, when assuming an autocorrelation of 0.5, a longer autocorrelation length means that dune development along a longer stretch of coast has an autocorrelation of that value. With higher autocorrelation lengths, dune development along the coast is thus more similar.

## 4. Results

### 4.1. Simplified building: Results from Scanex2020 (order 100 m)

During Scanex2020, the evolution of the beach around two containers and the dune toe were measured from the end of January until April 2020 (Fig. 8). The winds in this period are mainly from the southwest with maximum wind speeds over 20 m/s in the first month and with weaker winds coming from the east (Fig. 3) in the last two months. In the first month, a horseshoe-like deposition pattern (see also Poppema et al., 2021) develops in the lee (NNE side) of the container. This deposition pattern is indicated with two black lines in Fig. 8E, and the container is indicated with a black square in all subplots. The lobes develop into 20-m long stretches of deposition and reach heights of up to 50 cm. In the following months (Fig. 8F-H), the seaward lobe extends 10 m in length and increases in elevation in the first 10 m behind the container. The dune-ward lobe does not show any significant development after February 2020.

The influence of the container on the local sand transport over the 3-month period can be seen in Fig. 8H, which shows two clear downwind depositions behind the container. However, there doesn't seem to be any

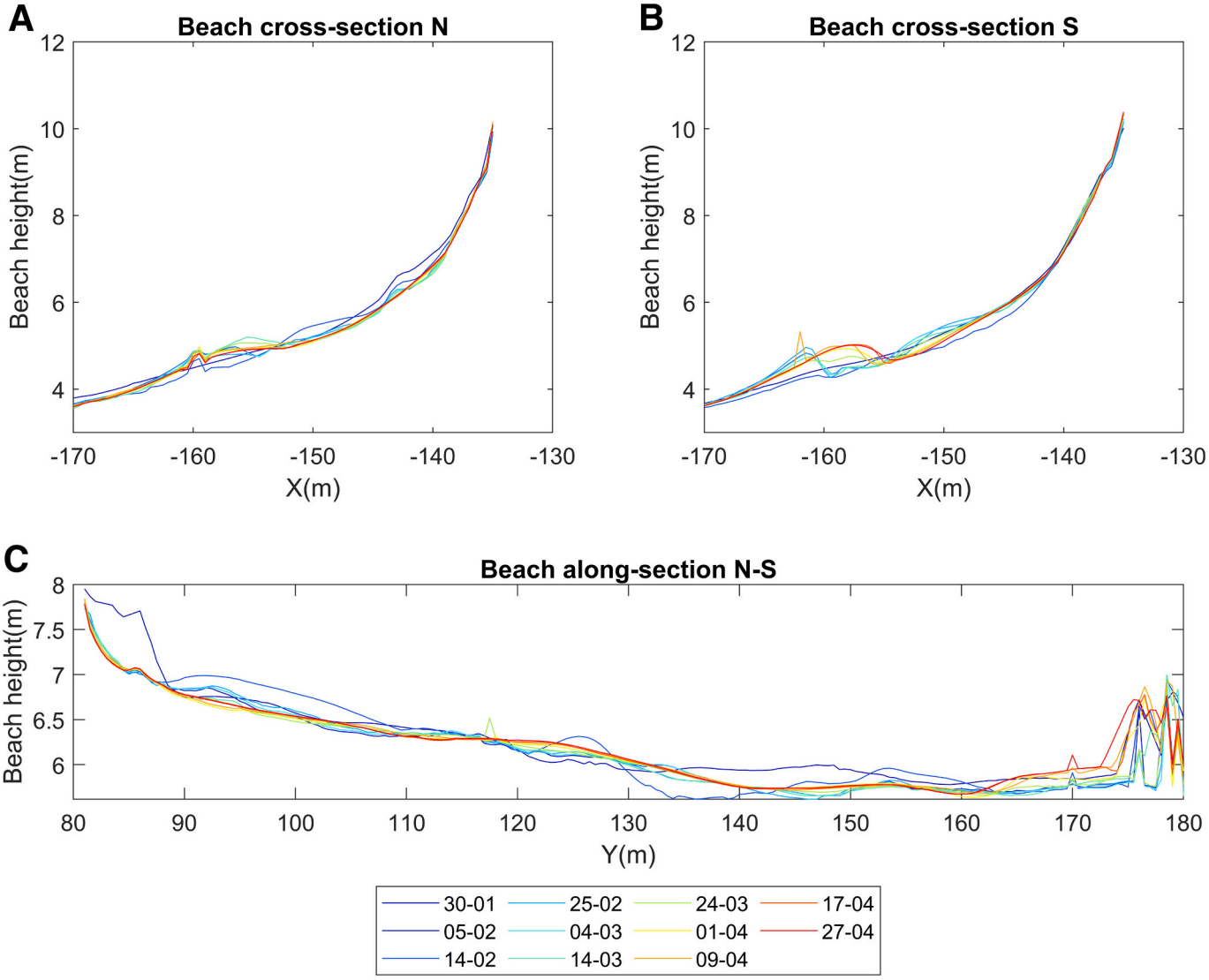


**Fig. 9.** Beach/dune cross-sections around the container during Scanex2020. The top plots show the cross-shore beach-dune profile (A) north and (B) south of the container while the bottom plot (C) shows the surface elevation development along the dune toe behind the container. The locations of the cross-sections are shown in Figs. 4B and 8.

persistent erosional/depositional trends caused by the presence of the container during the 3- month Scanex2020 campaign. This can also be seen in Fig. 9 which shows the height evolution along three profiles; two cross-shore profiles to the north and south of the container and one profile along the dune toe (X = −140 m).

### 4.2. Single building in front of dune: Results from the CoastScan experiment (order 500 m)

A larger perspective of the beach-dune development during Scanex2020 can be seen in Fig. 10 which shows the morphologic developments along 400 m of the beach-dune front around BP6 (indicated with black filled polygon). It shows the area is both influenced by aeolian wind driven sediment transport and anthropogenic factors. Examples of anthropogenic factors can be seen in; 1) Fig. 10B which shows a fan pattern on the southern side of BP6 (X = −175 m, Y = −175 m) due to bulldozing of a beach entrance, 2) Fig. 10D which shows sand clearing around BP6 (indicated with the blue colour) and 3) the same plot which shows the creation of a sand embankment in front of the BP6 as a storm protection (X = −220,Y = −0).

Aeolian effects can be seen at various locations around the beach pavilion. On the seaward side in Fig. 10B, D and F ripples perpendicular to the coast can clearly be seen. These are sand strips with an average wavelength of 12–17 m and, heights in the order of 5–10 cm, generated during wind conditions over 7 m/s (van IJzendoorn et al., 2024). South and east of BP6 (around Y = −50 < −>0 m, X = −150 m in Fig. 10B) sand accumulates at several locations around and in front of the dune toe forming part of the horseshoe deposition areas (indicated with black line). Especially between the beach pavilion and the dune front, considerable volumes of sand accumulate during the period, although almost all is removed quite quickly to keep the road behind the pavilion usable for motorized traffic. Sand is transported south of BP6 or dumped along the waterline. Just north of the beach pavilion (around X = −150 m, Y = 50 m, indicated with a black line), a horseshoe deposition pattern develops in the first month, but this disappears after the first month due to beach reshaping. Due to the same beach shaping no clear patterns develop after February 2020.

The patterns found during the Scanex2020 field experiment around BP6 result only locally (in time and space) in dune toe changes but due to constant reshaping longer term effects are hard to see within the three-month period. Results can only be seen more clearly over longer time periods like the CoastScan measurement period of two years. Fig. 11 shows two years of dune development (along the cross-sections indicated in Fig. 4E) north and south of BP6. The top of the primary dune in the southern profile (Fig. 11D) shows a progressive increase of about 1 m in two years while the profile development around the northern (Fig. 11C) dune top is more variable. Here, an increase of the dune profile height of about 50 cm is observed in the two years. On average, the dune height increases twice as fast on the southern side (0.5 m/y) than on the northern side of BP6 (0.25 m/s), although the growth is more irregular on the north side.

### 4.3. Multiple beach pavilions along Noordwijk beach: Results from aerial lidar measurements (order >1000 m)

The effect of multiple beach pavilions at Noordwijk beach can be seen in Fig. 12 which shows the dune development in height and volume over the last 15 years. The dune height is determined along the blue line shown in Fig. 7 while the volume is determined in the cross-shore direction between the two red lines.

The alongshore locations of the beach pavilions are indicated in Fig. 12A along with the seasonal or permanent status. The next Fig. 12 (B) shows the dune top height evolution along the 2.7-km beach dune system at Noordwijk. It starts from an approximately equal dune height in 2008 to dune heights varying between 9 and 16 m after 15 years of dune development. The dune height growth in this period varies between −20 % attributed to beach cleaning (personal communication water board Rijnland, The Netherlands) and + 200 % attributed to aeolian transport compared to the dune heights in 2008. The dune height drops regularly to a stable height of about 6–8 m at beach access paths and shows (seen from south to north) slopes in the dune height at various locations. The bottom of the slopes coincides at various locations with the locations of BPs, but this is not consistent. Slopes start for example at approximately Y = −850, −550 and 0 m in the neighborhood of BP2, BP4 and BP6 while BP3 and BP7 don't seem to create a big dip in the slope. Above Y = 400 m the pattern appears more irregular.

Dune volumes in Fig. 12C show a somewhat different trend. The initial dune volumes varied between 500 and 800 $m^3$ in 2008 (it should be noted that all calculations presented are made with the dune top/toe definition of 2023) and increased with a maximum of 200 $m^3$/m for the highest dunes, which is a 30 % volume increase since 2008. Dune volume variations follow a similar pattern as the height variations and relate similarly to the locations of beach buildings. Dune heights grow an averaged maximum of 0.5 m a year while dune volume growth reaches averaged volumes of up to 10-12 $m^3$ per meter per year. These values align with the values found around BP6 in the medium scale experiment. Fig. 12D and E show the average dune growth in dune height and volume with a black line and the standard deviation in red.

To study the variability of the dune properties, the autocorrelation (de Vries et al., 2012) of the dune height and volume is determined along the dune tops (see Fig. 7). Fig. 13 shows that the autocorrelation halves after 40–50 m while it drops to low numbers after 70–80 m. In time (2008- > 2023), the autocorrelation length also reduces, namely from 50 m (2008–2013) to about 20 m (2018–2023) for a correlation of 0.5. This corresponds to the dunes getting peakier through time (as seen in Fig. 12).

The BPs have different effects on the dune development downwind. Fig. 14 shows the average dune height development over the 2008–2023 period on the leeward side of the buildings (here the distance is measured downwind from the south side of each BP in north easterly direction). The results are presented in three groups with two groups showing similar trends and the last group showing the irregular trends. The first two groups show approximate 'linear' growth behind the pavilions towards the northeast with either an average of 15 or 40 cm growth per year within the 100 m downwind of the pavilion. The 'linear' trends are mostly found in the southern part of the study site while the irregular patterns are more found in the northern part.

A cross correlation analysis of the dune growth properties against the BP properties is shown in Fig. 15. The scatterplots show the average dune growth (in height/volume) against the distance between the BPs. The size of the scatter is proportional to the cross shore area of a BP (height*width) with larger buildings indicated by larger dots while the seasonal/permanent status is indicated by squares/dots (S/P in the legend).

The left plot shows the yearly height increase 100 m downwind of the BPs (like in Fig. 14) and shows some relation between the average dune height growth and a BP distance of 150 m. The status and size of the BP's show no clear relation to the dune height growth. The right plot shows the yearly dune volume increase over the first 100 m behind the BP and shows a somewhat similar relation of the dune volume increase with a BP distance of 150 m. Also, no clear correlations are seen regarding the status and size of the BPs.

## 5. Discussion

In this study, we looked at the effect of standalone beach buildings on monthly to decadal scale dune development. The results indicate that around individual beach buildings horseshoe depositions patterns develop which follow the mean wind direction on monthly time scales. However, due to constant human activities, like bulldozing, on the beach more persistent deposition patterns disappear. On a decadal time scale, dunes develop non-uniformly with large variations in dune

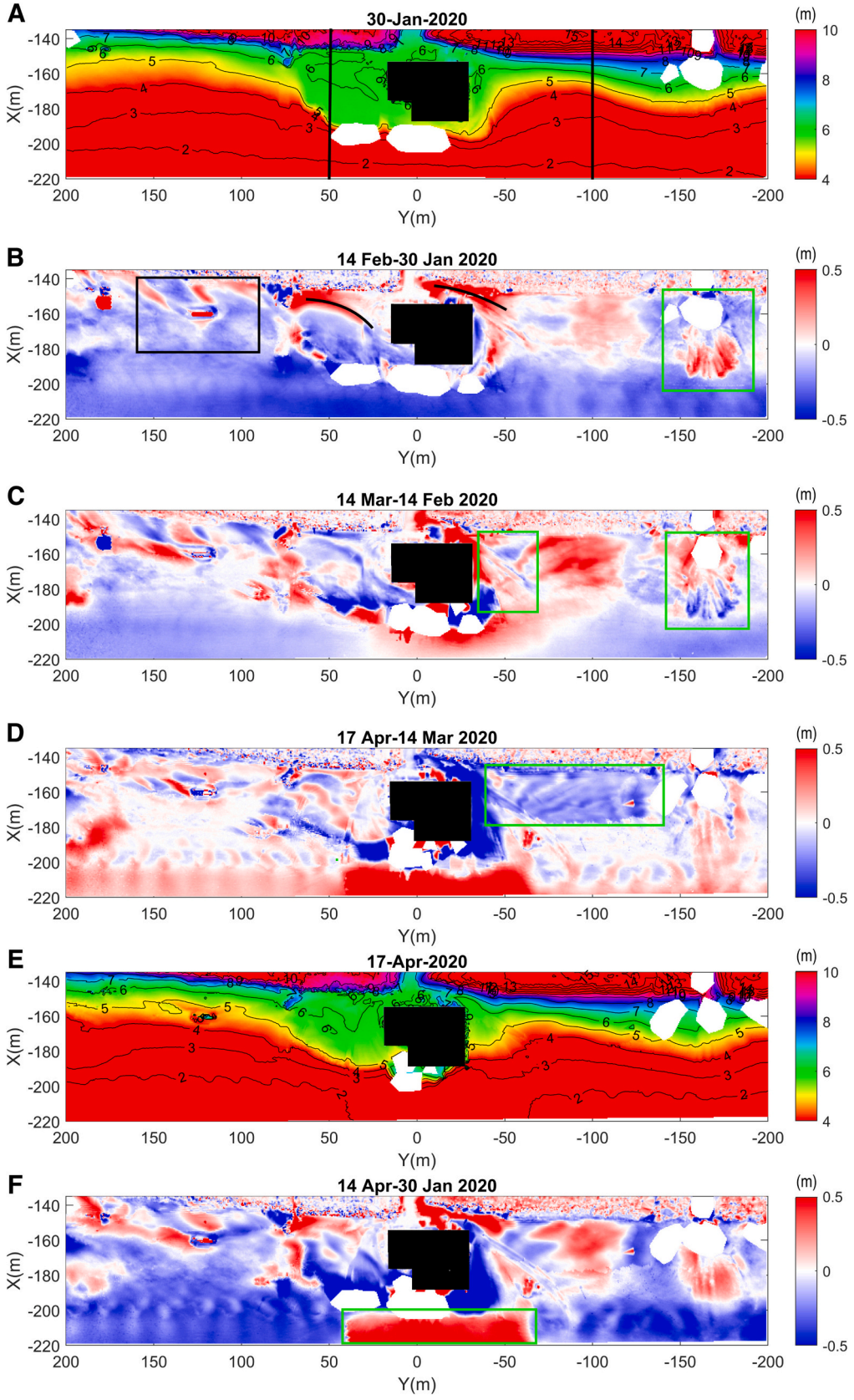


**Fig. 10.** Beach/dune height development around BP6 (black polygon) in 2020. Plots 10A and 10E show the height map for the first and last month of the 3-month Scanex2020 field campaign, while plots 10B-10D show consecutive monthly height differences in meters. The last plot 10F shows the height difference over the full study period. The black rectangular polygon (10B) indicates the field site around the container (see Figs. 4 and 8), the curved black lines (10B) show the initial depositions around BP6 while the vertical lines in 10A correspond to the cross-sections in Fig. 4. Green areas indicate areas with anthropogenic activities like beach cleaning or beach shaping. Data in the plots is triangulated with a maximum lag length of 10 m.

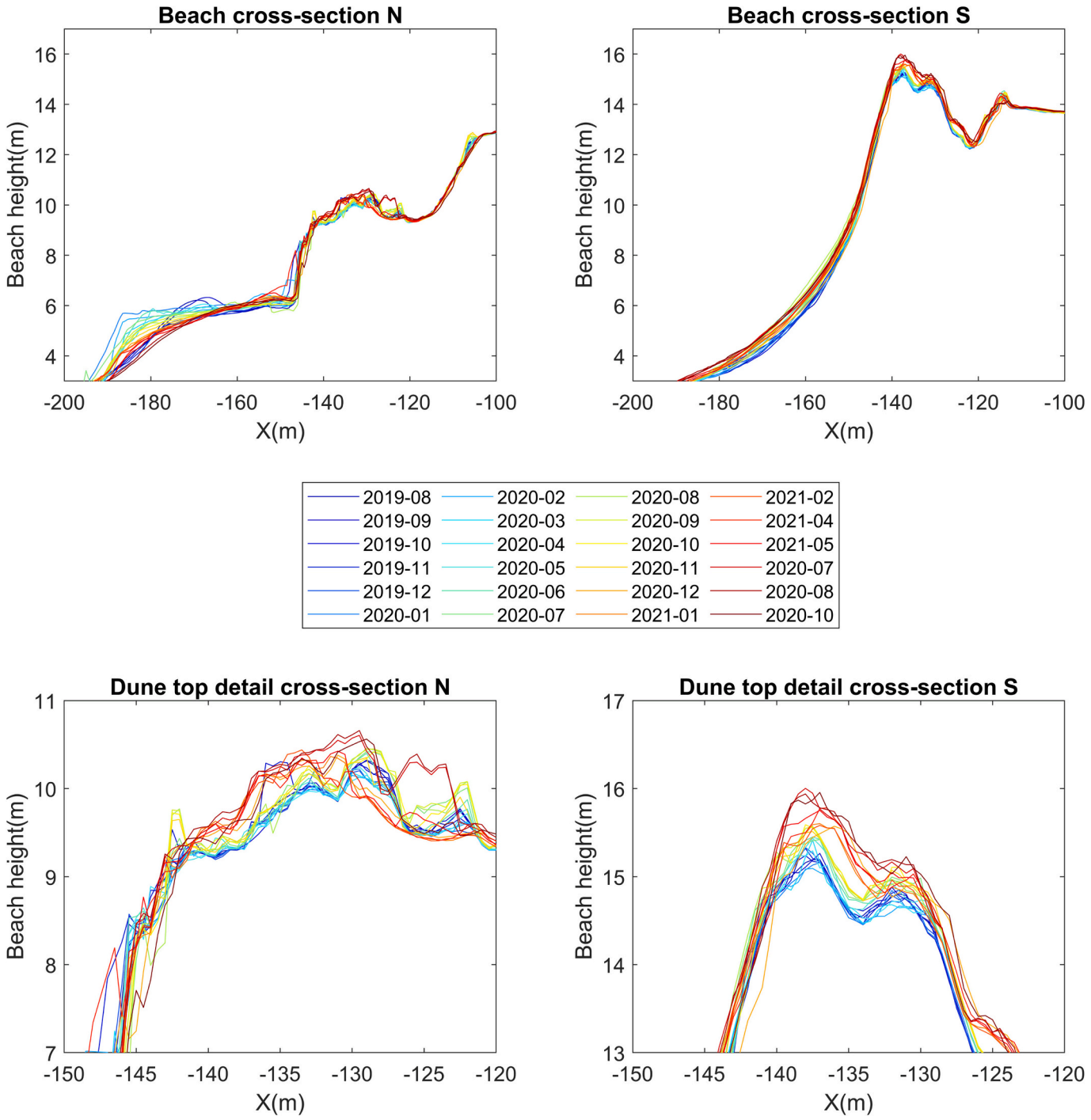


**Fig. 11.** Cross-section evolution north and south of BP6 (see Fig. 3). The top plots 10A and 10B show the dune development of the primary dune while the lower plots 10C and 10D show a detail of the dune top where dune growth is maximal.

height/volume growth when beach buildings are present.

Both small-scale and medium-scale measurements in this research show deposition patterns that form in the lee of a building. These deposition patterns have also been observed by Poppema et al. (2021) and are similar to deposition patterns around cuboid buildings (Hunt, 1971; Meroney et al., 1999; Schulman et al., 2000). The asymmetrical shape of the deposition patterns is similar to the numerical simulations of Pourteimouri et al. (2022) which show that these patterns develop when the wind hits a cuboid under an angle. The constant anthropogenic activities on the beach inhibit direct distinction of the effect of beach buildings on local dune development. For example, the depositions patterns around the building in the medium-scale measurements are bulldozed and development of the dune on the south side is affected by the presence of a beach entrance path.

Identifying any patterns in the influence of the individual buildings has been a challenge. Various statistical clustering techniques (like hierarchical clustering (Murtagh and Contreras, 2017) or K-means and DBSCAN (Kuschnerus et al., 2021)) produced little useful results. Due to the limited number of elements and the irregular length of these elements, obtained clusters show little significance. Only a manual grouping showed similar dune height patterns for about half of the beach pavilions. An analysis of these patterns with beach pavilions

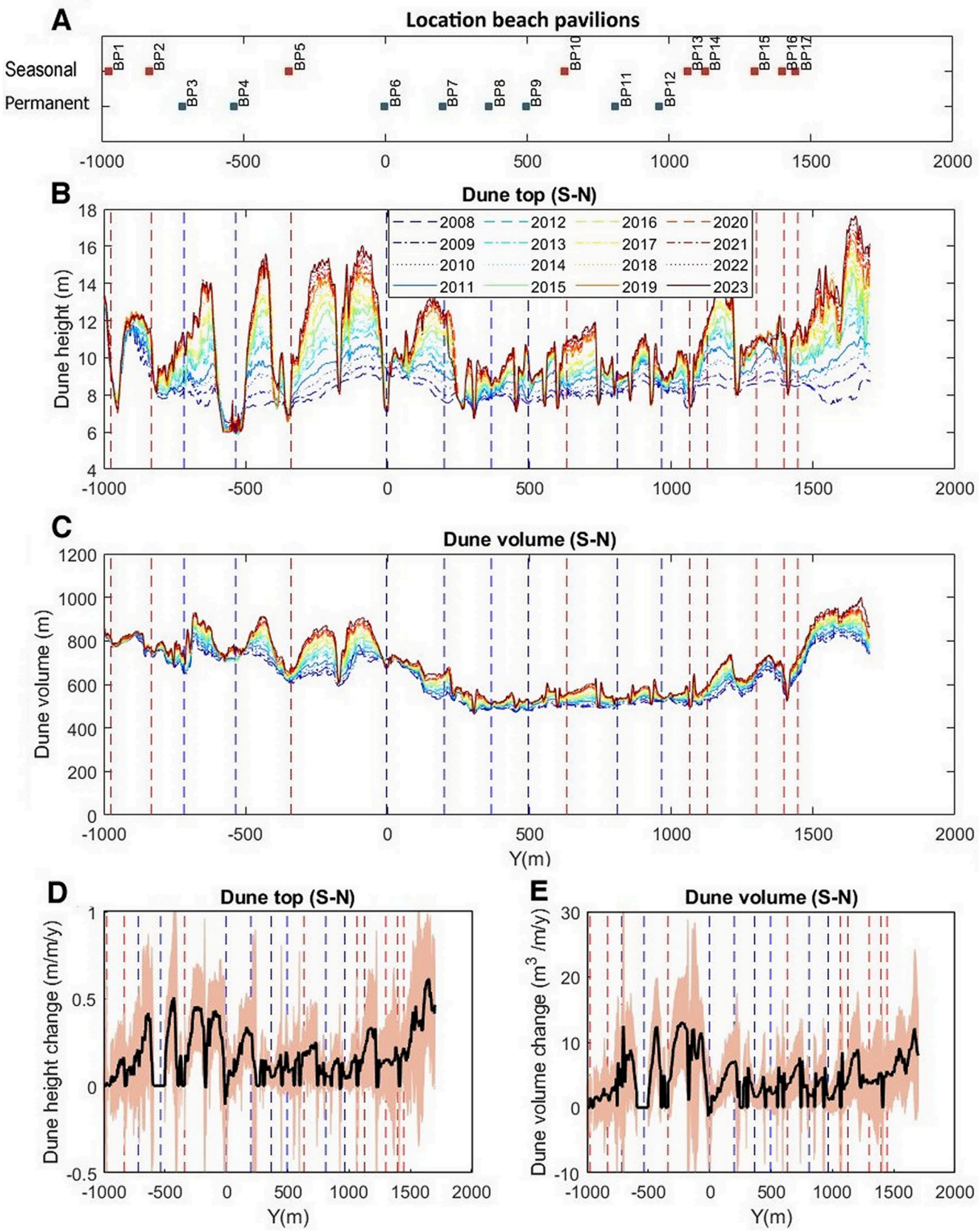


**Fig. 12.** Dune development along the Noordwijk coast with (A) the alongshore locations of the seasonal/permanent beach pavilions, (B) the dune height development (along the dune top line defined in Fig. 7) from 2008 until 2023 with the locations of the BPs as red/blue lines and (C) the dune volume development during the same period. Panels D and E s show the average height/volume change per year indicated in black and the standard deviation shaded in red.

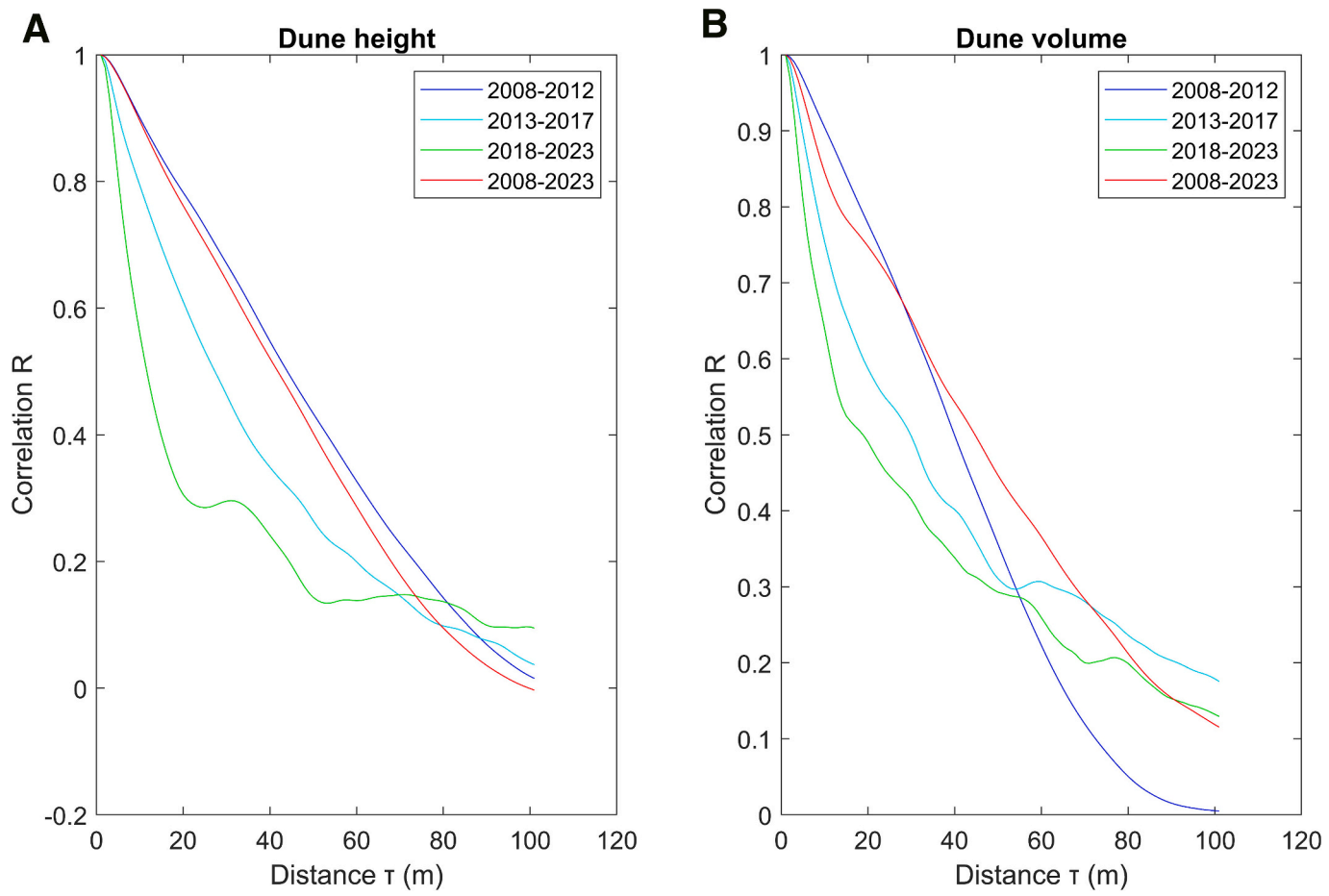


**Fig. 13.** Alongshore autocorrelation R of the dune height and volume along the dune top line (Fig. 4) for the three periods 2008–2012, 2013–2017, 2018–2023 and the total survey period 2008–2023.

characteristics (like distance between buildings and seasonal/permanent status) shows no clear correlations. Variations in the anthropogenic activities around each building might provide an alternative explanation for the differences in dune development patterns.

To better understand the effect of buildings on longer term dune development, it is important to obtain more information on both beach pavilion characteristics and anthropogenic actors. The effect of beach buildings cannot be distinguished clearly from event-driven beach shaping for path cleaning and pavilion sand embankments in the available datasets. Additional measurements are needed (like additional video data in Barbero-García et al., 2023) to correlate and distinguish natural and anthropogenic processes. This should provide answers to how (event driven) monthly variations around BPs translate into multi-year dune development. Also, more observations directly around BPs can provide new information about the complex aeolian/morphological/anthropogenic processes interacting near buildings, situated around the dune toe and their contribution to extreme local variations. Lastly more continuous long term datasets, as opposed to the present three separate datasets with various spatio-temporal scales, may help to understand the processes at various scales more clearly and understand their effect on the longer term. This would also allow for more advanced analysis techniques like 4D objects-by-change (Anders et al., 2020) to detect changes and relations over all relevant scales."

The maximum dune volume increase rates (up to 12 m3) in the study area are similar to other dunes in the Netherlands (de Vries et al., 2012) and Belgium (Strypsteen et al., 2019). However, the autocorrelation length for alongshore dune height and volume in the Noordwijk beach-dune system is 50 m for a correlation of 0.5, whereas for natural dunes in the Netherlands this value lies around 500 m (de Vries et al., 2012). This indicates that alongshore dune heights and volumes can vary significantly where buildings are present. Non-uniform dune development, as seen in Noordwijk, can influence the coastal resilience in the long run. If dune height and volume cannot keep up with expected rising sea level due to buildings and other anthropogenic effects coastal resilience can decrease significantly. With increasing worldwide urbanization (Kundu and Pandey, 2020) and sea level rise due to global climate change (IPCC, 2021) these problems can pose increased challenges for sandy coasts in the future.

## 6. Conclusions

A total of three different datasets at complementary spatio-temporal scales has been studied to determine the effect of buildings and other anthropogenic influences (such as beach shaping) on long term dune development on an urbanized beach in the Netherlands.

On small spatio-temporal scales (Order 100 m and weeks/months), the effects of beach buildings/containers and anthropogenic effects on Noordwijk beach can be distinguished, although the effect on the dune (toe) seems not easily detectable. Longer temporal scales in the order of years are needed to clearly detect effects on the dunes. The longer-term analyses (2 and 15 year) show large variations in dune height/volume growth along the urbanized beach of Noordwijk. Maximum dune volume growth rates (up to 12 $m^3/m/y$) are similar to other locations along the Dutch coast, but near buildings these rates can locally drop to almost zero.

Autocorrelation analysis shows that the alongshore variability of the dune height of an urbanized beach can be a factor 10 smaller than for natural beaches. A grouping of dune height profiles in the leeward side

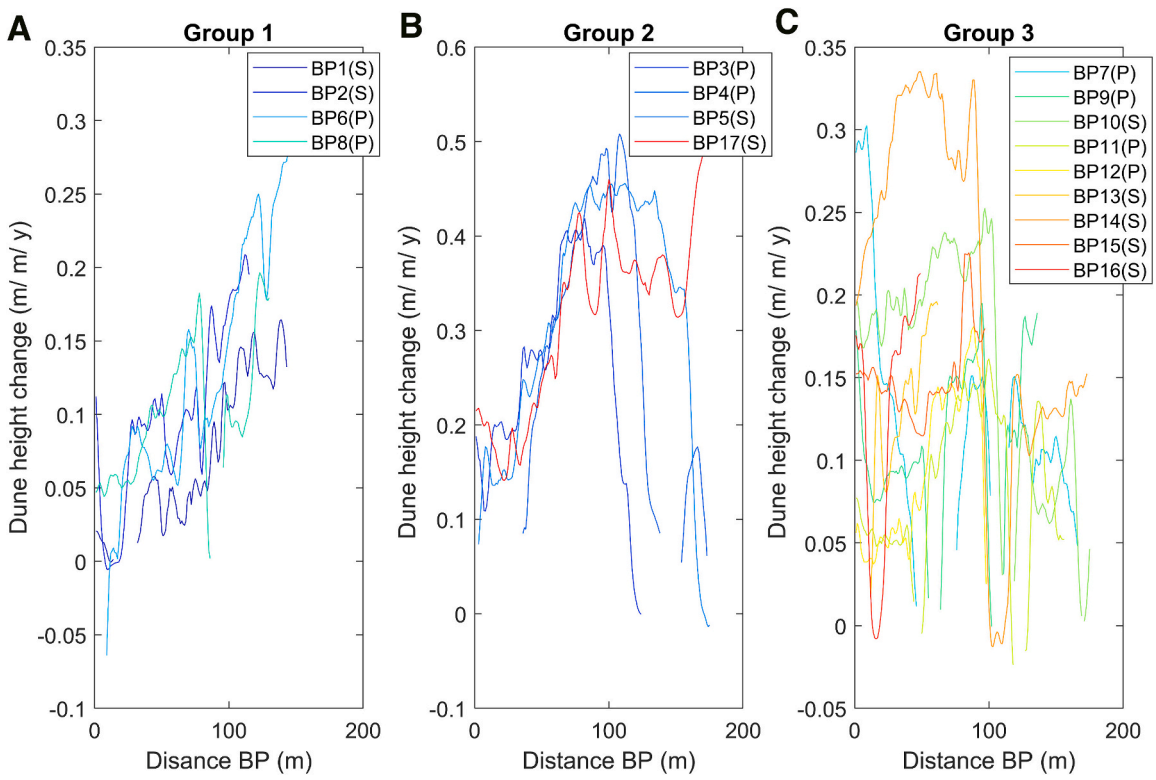


**Fig. 14.** Average dune growth per year on the leeward side of the BPs. Results are grouped in profiles with similar trends. The status of the BPs is indicated in the legend ('S' for seasonal and 'P' for permanent).

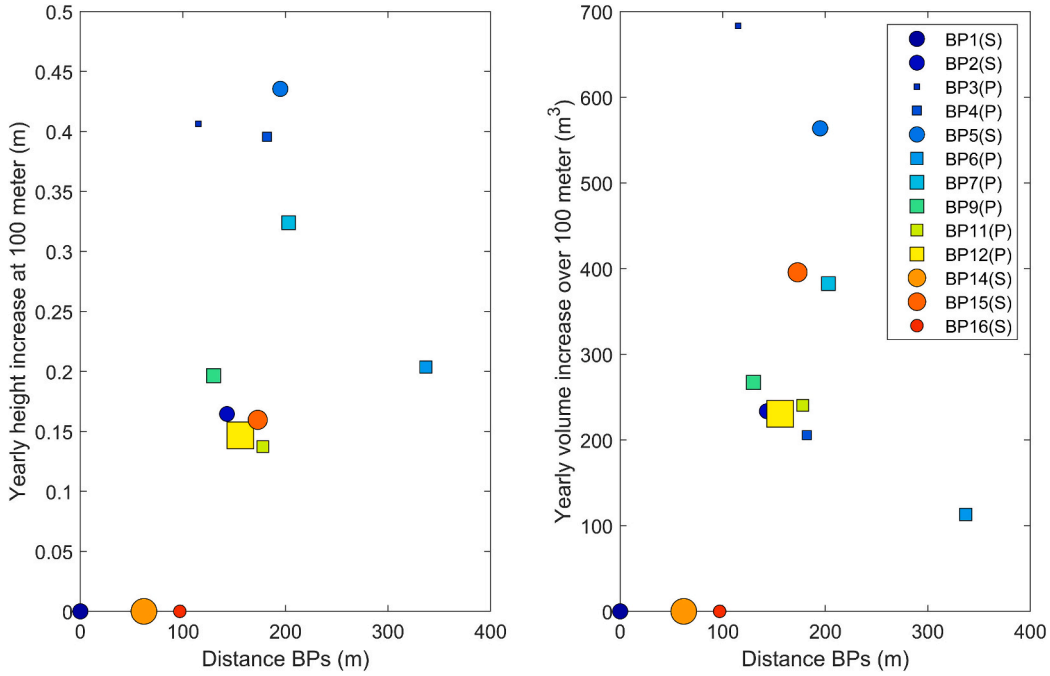


**Fig. 15.** Scatterplot of the yearly dune growth at 100 m/yearly volume increase over 100 m downwind of the BPs and the distance between the BPs. The status (seasonal/permanent) is indicated by squares/circles (S/P in the legend) and the size of the dots is proportional to the size (height*width) of the BP.

of the beach pavilions reveals two clear patterns (with increases of 0.15–0.4 m in dune height per 100 m length) for about halve the beach pavilions, but a clear pattern for all beach pavilions together cannot be distinguished. In the long term, the results indicate that anthropogenic activities on an urbanized beach can result in irregular dune development which can possibly reduce the natural resilience against climate change effects.

## CRediT authorship contribution statement

**Sander Vos:** Writing – review & editing, Writing – original draft, Visualization, Validation, Software, Resources, Project administration,

Methodology, Investigation, Funding acquisition, Formal analysis, Data curation, Conceptualization. **Christa van IJzendoorn:** Writing – review & editing, Writing – original draft, Methodology, Conceptualization. **Roderik Lindenbergh:** Writing – review & editing, Funding acquisition. **Alain de Wulf:** Writing – review & editing, Software, Funding acquisition.

## Declaration of competing interest

The authors declare the following financial interests/personal relationships which may be considered as potential competing interests: Sander Vos reports a relationship with Baars-CIPRO that includes: employment. Christa van Ijzendoorn reports a relationship with Delft University of Technology that includes: employment. If there are other authors, they declare that they have no known competing financial interests or personal relationships that could have appeared to influence the work reported in this paper.

## Data availability

Data with the article is available at www.doi.org/10.4121/05477395-f4fe-46dc-bed9-89da04c073cd

## Acknowledgements

The work in this article was partly financed by the Dutch ERC-Advanced grant 291206-Nearshore Monitoring and Modeling, the CoastScan (2018/STW/00505023) and Duneforce (2018/NWO/17064) project, contract 4500277210/31141555 of Rijkswaterstaat, Ministry of Infrastructure and Water Management, and finally Ghent University (Prof. Alain de Wulf), Belgium. The authors wish to thank the owner and manager of the Grand Hotel Huis ter Duin (https://huisterduin.com/) for supporting the research by allowing the use of the hotel infrastructure for the permanent TLS setup. Additional thanks go to Baars-CIPRO (www.baars-cipro.nl) for construction of the measuring frame and financial and operational support, Mieke Kuschnerus for providing fieldwork support, Daan Poppema for additional references and Joost Veer from waterboard Rijnland (The Netherlands) for providing information about the beach policies, beach/dune cleaning and beach pavilion characteristics.

## References

Almarshed, B., Figlus, J., Miller, J., Verhagen, H.J., 2020. Innovative coastal risk reduction through hybrid design: combining sand cover and structural defenses. J. Coast. Res. 36, 174–188. https://doi.org/10.2112/JCOASTRES-D-18-00078.1.

Anders, N., Valente, J., Masselink, R., Keesstra, S., 2019. Comparing filtering techniques for removing vegetation from UAV-based photogrammetric point clouds. Drones 3, 61. https://doi.org/10.3390/drones3030061.

Anders, K., Winiwarter, L., Lindenbergh, R.C., Williams, J.G., Vos, S.E., Höfle, B., 2020. 4D objects-by-change: spatiotemporal segmentation of geomorphic surface change from LiDAR time series. ISPRS J. Photogramm. Remote Sens. 159, 352–363. https://doi.org/10.1016/j.isprsjprs.2019.11.025.

Barbero-García, I., Kuschnerus, M., Vos, S.E., Lindenbergh, R.C., 2023. Automatic detection of bulldozer-induced changes on a sandy beach from video using YOLO algorithm. Int. J. Appl. Earth Obs. Geoinf. 117 https://doi.org/10.1016/j.jag.2023.103185.

Chehata, N., David, N., Bretar, F., 2008. LIDAR data classification using hierarchical K-means clustering. In: The International Archives of the Photogrammetry, Remote Sensing and Spatial Information Sciences: Beijing, Vol. XXXVII. Part B3b, pp. 325–330.

Coveney, S., Fotheringham, A.S., 2011. Terrestrial laser scan error in the presence of dense ground vegetation. Photogramm. Rec. 26, 135. https://doi.org/10.1111/j.1477-9730.2011.00647.x.

Dandois, J.P., Ellis, E.C., 2013. High spatial resolution three-dimensional mapping of vegetation spectral dynamics using computer vision. Remote Sens. Environ. 136, 259–276. https://doi.org/10.1016/j.rse.2013.04.005.

de Bruijne, A., van Buren, J., Kösters, A., van der Marel, H., 2005. Geodetic reference frames in the Netherlands, Definition and specification of ETRS89, RD and NAP, and their mutual relationships. In: Netherlands Geodetic Commission 43, Delft, p. 132 (ISBN 90 6132291 X).

de Vries, S., Southgate, H.N., Kanning, W., Ranasinghe, R., 2012. Dune behavior and aeolian transport on decadal timescales. Coast. Eng. 67, 41–53. https://doi.org/10.1016/j.coastaleng.2012.04.002.

De Winter, R.C., Gongriep, F., Ruessink, B.G., 2015. Observations and modeling of alongshore variability in dune erosion at Egmond aan Zee, the Netherlands. Coast. Eng. 99, 167–175. https://doi.org/10.1016/j.coastaleng.2015.02.005.

Diamantidou, E., Santinelli, G., Giardino, A., Stronkhorst, J., de Vries, S., 2020. An automatic procedure for dune foot position detection: application to the Dutch coast. J. Coast. Res. 36, 668. https://doi.org/10.2112/JCOASTRES-D-19-00056.1.

Evans, J.S., Hudak, A.T., 2007. A multiscale curvature algorithm for classifying discrete return LiDAR in forested environments. IEEE Trans. Geosci. Remote Sens. 45, 1029–1038. https://doi.org/10.1109/tgrs. 2006.890412.

Flor-Blanco, G., Flor, G., Pando, L., 2013. Evolution of the Salinas-El Espartal and Xagó beach/dune systems in North-Western Spain over recent decades: evidence for responses to natural processes and anthropogenic interventions. Geo-Mar. Lett. 33, 143–157. https://doi.org/10.1007/s00367-012-0301-3.

García-Romero, L., Hernández-Cordero, A.I., Fernández-Cabrera, E., Peña-Alonso, C., Hernández-Calvento, L., Pérez-Chacón, E., 2016. Urban-touristic impacts on the aeolian sedimentary systems of the Canary Islands: conflict between development and conservation. Island Stud. J. 11, 91–112. https://doi.org/10.24043/isj.336.

Hallin, C., Huisman, B., Larson, M., Walstra, D.J., Hanson, H., 2019. Impact of sediment supply on decadal-scale dune evolution — analysis and modelling of the Kennemer dunes in the Netherlands. Geomorphology 337. https://doi.org/10.1016/j.geomorph.2019.04.003.

Hallin, C., van IJzendoorn, C., Homberger, J.M., de Vries, S., 2023. Simulating surface soil moisture on sandy beaches. Coast. Eng. 185, 104376 https://doi.org/10.1016/j.coastaleng.2023.104376.

Hantson, W., Kooistra, L., Slim, P.A., 2012. Mapping invasive woody species in coastal dunes in the Netherlands: a remote sensing approach using LIDAR and high-resolution aerial photographs. Appl. Veg. Sci. 15, 536–547. https://doi.org/10.1111/j.1654-109X.2012.01194.x.

Hesp, P., 1989. A review of biological and geomorphological processes involved in the initiation and development of incipient foredunes. Proc. R. Soc. Ed. Sect. B: Biol. Sci. 96, 181–201. https://doi.org/10.1017/S0269727000010927.

Hesp, P.A., Walker, I.J., 2013. Coastal dunes. In: Shroder, J.F. (Ed.), Treatise on Geomorphology. Elsevier, London, pp. 328–355.

Hoonhout, B., de Vries, S., 2017. Aeolian sediment supply at a mega nourishment. Coast. Eng. 123, 11–20. https://doi.org/10.1016/j.coastaleng.2017.03.001.

Hoonhout, B., van Thiel de Vries, J., 2013. Invloed van strandbebouwing op zandverstuiving: adviezen voor vergunningverlening, Deltares, Technical Report, p. 42 (open.rijkswaterstaat.nl/open-overheid/onderzoeksrapporten/@135711/invloed-strandbebouwing-zandverstuiving/).

Hoonhout, B.M., Waagmeester, N., 2014. Influence on Beach Buildings on Aeolian Sand Transport, an Inventarisation of Methods, Measurements and Models, Technical Report, Deltares, Delft.

Houser, C., 2013. Alongshore variation in the morphology of coastal dunes: Implications for storm response. Geomorphology 199, 48–61. https://doi.org/10.1016/j.geomorph.2012.10.035.

Huang, Y., Jin, P., 2018. Impact of human interventions on coastal and marine geological hazards: a review. Bull. Eng. Geol. Environ. 77, 1081–1090. https://doi.org/10.1007/s10064-017-1089-1.

Hunt, J., 1971. The effect of single buildings and structures. Philos. Trans. R. Soc. 269 (1199), 457–467.

Intergovernmental Panel on Climate Change (2021: Summary for policymakers. In: Climate Change 2021: The Physical Science Basis. Contribution of Working Group I to the Sixth Assessment Report of the Intergovernmental Panel on Climate Change [Masson-Delmotte, V., P. Zhai, A. Pirani, S.L. Connors, C. Péan, S. Berger, N. Caud, Y. Chen, L. Goldfarb, M.I. Gomis, M. Huang, K. Leitzell, E. Lonnoy, J.B.R. Matthews, T. K. Maycock, T. Waterfield, O. Yelekçi, R. Yu, B. Zhou], (In Press).

Jackson, N.L., Nordstrom, K.F., 2011. Aeolian sediment transport and landforms in managed coastal systems: a review. Aeolian Res. 3, 181–196. https://doi.org/10.1016/j.aeolia.2011.03.011.

Kathmann, H.S., van Natijne, A.L., Lindenbergh, R.C., 2022. Probabilistic vegetation transitions in dunes by combining spectral and lidar data. In: ISRPS, International Archives of Photogrammetry, Remote Sensing and Spatial Information Sciences, XLIII-B2-2022, pp. 1033–1040. https://doi.org/10.5194/isprs-archives-XLIII-B2-2022-1033-2022.

KNMI (Koninklijk Nederlands Meteorologisch Instituut), 2024. Weather data at IJmuiden, The Netherlands. Available online: https://www.daggegevens.knmi.nl/klimatologie/uurgegevens. Station 225, Last visited on 8-4.

Kundu, D., Pandey, A.K., 2020. World urbanisation: trends and patterns. In: Kundu, D., Sietchiping, R., Kinyanjui, M. (Eds.), Developing National Urban Policies. Springer, Singapore. https://doi.org/10.1007/978-981-15-3738-7_2.

Kuschnerus, M., Lindenbergh, R.C., Vos, S.E., 2021. Coastal change patterns from time series clustering of permanent laser scan data. Earth Surf. Dyn. 9, 89–113. https://doi.org/10.5194/esurf-9-89-2021.

Kuschnerus, M., Lindenbergh, R.C., Vos, S.E., Hanssen, R., 2023. Statistically Assessing Vertical Change on a Sandy Beach from Permanent Laser Scanning Time Series, IRPS, International Archives of Photogrammetry, Remote Sensing and Spatial Information Sciences, 11. https://doi.org/10.1016/j.ophoto.2023.100055.

Luijendijk, A.P., Ranasinghe, R., De Schipper, M.A., Huisman, B.A., Swinkels, C.M., Walstra, D.J., Stive, M.J., 2017. The initial morphological response of the Sand Engine: a process-based modelling study. Coast. Eng. 119, 14. https://doi.org/10.1016/j.coastaleng.2016.09.005.

Malavasi, M., Santoro, R., Cutini, M., Acosta, A.T.R., Carranza, A.T.R., 2013. What has happened to coastal dunes in the last half century? A multitemporal coastal

landscape analysis in Central Italy. Landsc. Urban Plan. 119, 54–63. https://doi.org/10.1016/j.landurbplan.2013.06.012.
Masselink, G., Lazarus, E.D., 2019. Defining coastal resilience. Water 11. https://doi.org/10.3390/w11122587.
Masselink, G., Kroon, A., Davidson-Arnoot, R.G.D., 2006. Morphodynamics of intertidal bars in wave-dominated coastal settings: a review. Geomorphology 73, 33–49. https://doi.org/10.1016/j.geomorph.2005.06.007.
Meroney, R.N., Leitl, B.M., Rafailidis, S., Schatzmann, M., 1999. Wind-tunnel and numerical modeling of flow and dispersion about several building shapes. J. Wind Eng. Ind. Aerodyn. 81, 333–345. https://doi.org/10.1016/S0167-6105(99)00028-8.
Moran, P.A.P., 1950. Notes on continuous stochastic phenomena. Biometrika 37, 17–23. https://doi.org/10.2307/2332142.
Morton, R.A., Paine, J.G., Gibeaut, J.C., 1994. Stages and durations of post-storm beach recovery, southeastern Texas coast, USA. J. Coast. Res. 10 (4), 884–908.
Murtagh, F., Contreras, P., 2017. Algorithms for hierarchical clustering: an overview, II. Wiley Interdiscip. Rev.: Data Min. Knowl. Discovery 7 (6), e1219.
Nordstrom, K.F., 1994. Beaches and dunes of human-altered coasts. Prog. Phys. Geogr. 18, 497–516.
Nordstrom, K.F., McCluskey, J.M., 1985. The effects of houses and sand fences on the Eolian Sediment Budget at Fire Island, New York. J. Coast. Res. 1, 39–46.
Nordstrom, K.F., Jackson, N.L., Hartman, J.M., Wong, M., 2007. Aeolian sediment transport on a human-altered foredune. Earth Surf. Process. Landf. 1, 102–115. https://doi.org/10.1002/esp.1377.
Poppema, D.W., Wijnberg, K.M., Mulder, J.P.M., Vos, S.E., Hulscher, S.J.M.H., 2021. The effect of building geometry on the size of aeolian deposition patterns: scale model experiments at the beach. Coast. Eng. 168, 103866 https://doi.org/10.1016/j.coastaleng.2021.103866.
Poppema, D.W., Wijnberg, K.M., Mulder, J.P.M., Hulscher, S.J.M.H., 2022a. Deposition patterns around buildings at the beach: effects of building spacing and orientation. Geomorphology 401, 108–114. https://doi.org/10.1016/j.geomorph.2022.108114.
Poppema, D.W., Baas, A.C.W., Hulscher, S.J.M.H., Wijnberg, K.M., 2022b. Cellular automaton modelling of the effects of buildings on aeolian bedform dynamics. Aeolian Res. 59, 100840 https://doi.org/10.1016/j.aeolia.2022.100840.
Pourteimouri, P., Campmans, G.H.P., Wijnberg, K.M., Hulscher, S.J.M.H., 2022. A numerical study on the impact of building dimensions on airflow patterns and bed morphology around buildings at the beach. J. Mar. Sci. Eng. 10, 13. https://doi.org/10.3390/jmse10010013.
Pourteimouri, P., Campmans, G.H.P., Wijnberg, K.M., Hulscher, S.J.M.H., 2023. Modelling the influence of beach building pole heights on aeolian morphology and downwind sediment transport. Geomorphology 436, 108791. https://doi.org/10.1016/j.geomorph.2023.108791.
Riegl, 2023. Riscan Pro scan software (version 2.6.4, 64 bit), Provided with the laser scanner and obtainable via Riegl. www.riegl.com last visited 15-10.
RWS (Rijkswaterstaat, Ministry of Public Works), 2023. Data obtainable via. https://download.rijkswaterstaat.nl (Grid 24HZ1, 30EN2 and 30FN1), last visited 15-11.
Sallenger Jr., A.H., Krabill, W.B., Swift, R.N., Brock, J., List, J., Hansen, M., Holman, R. A., Manizade, S., Sontag, J., Meredith, A., Morgan, K., Yunkel, J.K., Frederick, E.B., Stockdon, H., 2003. Evaluation of airborne topographic lidar for quantifying beach changes. J. Coast. Res. 19, 125–133.
Schulman, L.L., Strimaitis, D.G., Scire, J.S., 2000. Development and evaluation of the PRIME plume rise and building downwash model. J. Air Waste Manage. Assoc. 50, 378–390. https://doi.org/10.1080/10473289.2000.10464017.
Strypsteen, G., Houthuys, R., Rauwoens, P., 2019. Dune volume changes at decadal timescales and its relation with potential aeolian transport. J. Mar. Sci. Eng. 7, 357. https://doi.org/10.3390/jmse7100357.
Tsoar, H., Blumberg, D.G., Stoler, Y., 2004. Elongation and migration of sand dunes. Geomorphology 57, 293–302.
van Bergen, J., Mulder, J., Nijhuis, S., Poppema, D., Wijnberg, K., Kuschnerus, M., 2021. Urban dunes: towards BwN design principles for dune formation along urbanized shores. Res. Urbanism Ser. 7, 101–128. https://doi.org/10.47982/rius.7.130.
van IJzendoorn, C.O., de Vries, S., Hallin, C., Hesp, A., 2021. Sea level rise outpaced by vertical dune toe translation on prograding coasts. Nat. Sci. Rep. 11, 12792 https://doi.org/10.1038/s41598-021-92150-x.
van IJzendoorn, C.O., Hallin, C., Cohn, N., Reniers, A.J.H.M., de Vries, S., 2023. Novel sediment sampling method provides new insights into vertical grain size variability due to marine and aeolian beach processes. Earth Surf. Process. Landf. 48, 782–800. https://doi.org/10.1002/esp.5518.
van IJzendoorn, C.O., Boomaars, K., Vos, S.E., Reniers, A.J.H.M., Kuschnerus, M., Lindenberg, R., 2024. Detection of Aeolian Sand Strips and their Characteristics Using Terrestrial Laser Scanning. Geomorphica. (in review).
Viborg, 1788. Efterretning om Sandvexterne og deres Anvendelse til at dæmpe Sandflugten paa Vesterkanten af Jylland. København. Text available via. https://archive.org/details/efterretningoms00vibogoog/page/n6/mode/2up.
Vos, S., Lindenbergh, R., de Vries, S., 2017. (2017) CoastScan: continuous monitoring of coastal change using terrestrial laser scanning. Proc. Coast. Dyn. 233, 1518–1528. https://coastaldynamics2017.dk/onewebmedia/233_Vos_Sander.pdf.
Vos, S.E., Spaans, L., Reniers, A., Holman, R., Mccall, R., de Vries, S., 2020. Cross-shore intertidal bar behavior along the Dutch Coast: laser measurements and conceptual model. J. Mar. Sci. Eng. 8, 864. https://doi.org/10.3390/jmse8110864.
Vos, S.E., Anders, K., Kuschnerus, M., Lindenbergh, R.C., Höfle, B., Aarninkhof, S.G.F., de Vries, S., 2022. A high-resolution 4D terrestrial laser scan dataset of the Kijkduin beach-dune system, The Netherlands. Nat. Sci. Data 9, 1–11. https://doi.org/10.1038/s41597-022-01291-9.
Vos, S.E., Kuschnerus, M., Lindenbergh, R.C., de Vries, S., 2023. 4D Spatio-temporal Laser Scan Dataset of the Beach-dune System in Noordwijk, NL (Version 1) [Data set], 4TU.ResearchData. https://doi.org/10.4121/1AAC46FB-7900-4D4C-A099-D2CE354811D2.V1.
Vos, S.E., van IJzendoorn, C., Lindenbergh, R.C., de Wulf, Alain, 2024. Combined datasets for article non-uniform dune development in the presence of standalone beach [Data set]. In: 4TU.ResearchData. https://doi.org/10.4121/05477395-f4fe-46dc-bed9-89da04c073cd.
Wernette, P., Thompson, S., Eyler, R., Taylor, H., Taube, C., Medlin, A., Decuir, C., Houser, C., 2018. Defining dunes: evaluating how dune feature definitions affect dune interpretations from remote sensing. J. Coast. Res. 34, 1460–1470. https://doi.org/10.2112/JCOASTRES-D-17-00082.1.
Wijnberg, K.M., 2002. Environmental controls on decadal morphologic behavior of the Holland coast. Mar. Geol. 189, 227–247. https://doi.org/10.1016/S0025-3227(02)00480-2.
Wijnberg, K.M., Poppema, D., Mulder, J.P.M., van Bergen, J., Campmans, G.H.P., Galiforni Silva, F., Hulscher, S., Pourteimouri, P., 2021. Beach-dune modelling in support of Building with Nature for an integrated spatial design of urbanized sandy shores. Res. Urban. Ser. 7, 241–260. https://doi.org/10.47982/rius.7.136.
Zhang, J., Lin, X., 2013. Filtering airborne LiDAR data by embedding smoothness-constrained segmentation in progressive TIN densification. ISPRS J. Photogramm. Remote Sens. 81, 44–59. https://doi.org/10.1016/j.isprsjprs.2013.04.001.